Vibrio parahaemolyticus quorum sensing controls phage VP882 transmission

Molly R. Sargen[1] and Bonnie L. Bassler[1,2]#

[1]Department of Molecular Biology, Princeton University, Princeton, New Jersey, United States of America

[2]Howard Hughes Medical Institute, Chevy Chase, Maryland, United States of America

#Address correspondence to Bonnie L. Bassler, bbassler@princeton.edu

Keywords: phage receptor, quorum sensing, superinfection, lysogeny

Abstract

Quorum sensing is a cell-to-cell communication process bacteria use to orchestrate collective behaviors. Quorum sensing involves the production, release, and detection of extracellular signal molecules called autoinducers. Some temperate phages can monitor bacterial autoinducers enabling them to track the abundance of potential host cells in the vicinity. Quorum-sensing-responsive phages can preferentially launch the transition from lysogeny to lytic replication at high cell density, presumably maximizing transmission. Once the phage lytic program is enacted, if nearby host cells are already lysogens, infections initiated by released virions could be nonproductive due to homoimmunity or superinfection exclusion mechanisms, posing a conundrum for temperate phages, including those that surveil quorum-sensing autoinducers. Here, we define host and phage components that influence transmission of the first discovered quorum-sensing-responsive phage, phage VP882, in populations of its host, *Vibrio parahaemolyticus*. We show that phage VP882 uses the K-antigen of serotype O3:K6 as its receptor. We demonstrate that host cells can prevent phage access to the O3:K6 K-antigen via

quorum-sensing-control of the export of polysaccharides that shield the K-antigen from the phage at high cell density. We discover that phage VP882 can superinfect and superlysogenize *V. parahaemolyticus*, overcoming the challenge of detecting whether or not potential hosts are lysogens. Following superlysogenization, recombination of the resident and newly infecting phage genomes can occur possibly promoting phage VP882 genome diversification.

Importance

A longstanding mystery is how temperate phages optimally time the launch of their lytic cascades to maximize spread. Quorum-sensing-responsive phages can preferentially execute their lytic replication programs at high host cell density, which in principle should foster transmission. However, if nearby host cells are already lysogens, infections initiated by released virions could be nonproductive due to homoimmunity or superinfection exclusion. We define host and phage components influencing transmission of the quorum-sensing-responsive phage VP882 in *Vibrio parahaemolyticus* populations. Phage VP882 uses the O3:K6 K-antigen as its receptor. Host cells prevent phage infection via quorum-sensing-controlled export of polysaccharides that shield the K-antigen at high cell density. We discover that phage VP882 can superinfect and superlysogenize *V. parahaemolyticus*, overcoming the challenge of detecting whether or not potential hosts are lysogens. These findings reveal how phages can capitalize on interception of host quorum-sensing cues to maximize their reproductive success.

Introduction

Temperate phages alternate between lytic and lysogenic lifestyles[1]. When a phage is lytic, it replicates, kills its current host cell, and spreads to new cells. During lysogeny, the phage establishes a stable relationship with its host and is transmitted vertically as a prophage. Transitioning between lytic and lysogenic lifestyles enhances phage reproductive success by maximizing the potential for transmission[2]. Theory and experimental evidence suggest that phage transmission through the lytic route is often favored when susceptible hosts are abundant while lysogeny is preferred when potential new hosts are rare[3,4]. Quorum sensing (QS) is a cell-to-cell communication process in which bacteria produce, release, and detect extracellular signal molecules called autoinducers. QS enables bacteria to orchestrate collective behaviors[5]. Some temperate phages can monitor host QS autoinducers, allowing them to estimate host cell abundance and launch the lytic cycle at high cell density when many host cells are present[6,7].

A conundrum all temperate phages face when launching the lytic cycle is whether host cells in the vicinal community are already infected or not. Encountering bacteria that are already lysogens is often a dead-end for a phage because the lytic repressor produced from the genome of the resident lysogenic phage suppresses transcription from the newly infecting phage[8,9]. This process is known as homoimmunity and is protective for both the bacterial host and the resident prophage[10]. In other cases, prophages encode superinfection exclusion mechanisms that prevent infection of already lysogenized cells[11,12]. Superinfection immunity often occurs through alteration of the expression or function of the phage receptor on the host cell surface[13–16]. Superinfection exclusion protects lysogenic host cells and, unlike in the case of homoimmunity, also preserves the population of free phage virions so they are available to infect naïve hosts[17].

69 Homoimmunity and superinfection exclusion mechanisms potentially threaten the reproductive
70 success of QS-responsive prophages that launch their lytic cycles at high cell densities.

71

72 Phage VP882, the first phage discovered to surveil a host QS autoinducer, infects the pathogen
73 *Vibrio parahaemolyticus*. *V. parahaemolyticus* has two QS systems (Figure 1). First, the VqmA-
74 VqmR QS pathway is controlled by the DPO autoinducer[18]. At high cell density, the VqmA
75 transcription factor binds DPO, and the DPO-VqmA complex activates expression of *vqmR*
76 encoding the VqmR small RNA (sRNA). VqmR promotes expression of genes required for group
77 behaviors. Second, the LuxO-driven QS cascade is responsive to three autoinducers that are
78 detected by three membrane bound receptors and, via a phosphorylation-dephosphorylation
79 cascade, the receptors modulate the activity of the LuxO transcription factor[5]. At low cell density,
80 LuxO is phosphorylated and it controls a regulon underpinning individual behaviors. At high cell
81 density, LuxO is dephosphorylated, and under this condition, the regulon responsible for group
82 traits is enacted.

83

84 The life cycle of phage VP882 is influenced by both the *V. parahaemolyticus* VqmA-VqmR[19] and
85 LuxO QS systems[6,20], both promoting lytic replication at high host cell densities. Specifically, the
86 phage VP882-encoded $VqmA_{Phage}$ receptor binds DPO[21] and DPO-$VqmA_{Phage}$ activates
87 transcription of *qtip* encoding Qtip, a small protein anti-repressor that sequesters and inactivates
88 cI, the phage VP882 lytic repressor[13]. Via an undefined mechanism, at high cell density, signaling
89 through the LuxO QS system increases phage VP882 lytic gene transcription[20] favoring lytic
90 replication over lysogeny[23].

91

92 If or how phage VP882 gauges the susceptibility of potential new host cells and whether
93 hommoimmunity or superinfection exclusion occurs have not been investigated. Toward an
94 understanding of those features, here we define factors that influence phage VP882 transmission.
95 We identify the receptor of phage VP882 as the O3:K6 K-antigen that is specific to its host strain.
96 We show that phage access to the O3:K6 K-antigen is controlled by LuxO-directed QS regulation
97 of a transport system responsible for export of polysaccharides that shield the K-antigen. QS-
98 mediated derepression of the genes encoding the transport system at high cell density prevents
99 phage VP882 adsorption and infection. We demonstrate that phage VP882 does not encode a
100 superinfection exclusion mechanism, so *V. parahaemolyticus* cells that are lysogenic for phage
101 VP882 can be infected by virions released from neighboring cells. Following superinfection, DNA
102 from newly infecting phages can recombine with the resident phage genome resulting in
103 superlysogenic conversion. We propose that QS-driven host superinfection via reliance on a
104 specific K-antigen receptor could foster phage VP882 genomic diversification in lysogenic *V.*
105 *parahaemolyticus* populations.

106 **Results**

107 **The O3:K6 K-antigen is the phage VP882 receptor in *V. parahaemolyticus***

108 A primary determinant of phage transmission concerns the ability of phage to attach to host cells.
109 In our continuing effort to define mechanisms that enable phage VP882 to propagate and to
110 connect those mechanisms to its capability to surveil host QS, we investigated phage VP882 host
111 range by identifying the *V. parahaemolyticus* phage receptor that enables infection. To do this,

112 we performed transposon mutagenesis on *V. parahaemolyticus* 882, the natural host of phage
113 VP882, that had been cured of the phage. We infected the pool of transposon insertion mutants
114 with phage VP882 and isolated colonies that were not killed (Figure 2A). The notion was that
115 surviving mutants were resistant to phage VP882 infection. Complicating this simple premise is
116 that phage VP882 is a temperate phage, so infection can result in either lytic replication or
117 lysogenization. Thus, following mutagenesis and infection, some host cells that survived could
118 have been lysogens. To overcome this issue, the strain we used for the transposon mutagenesis
119 carried a plasmid harboring arabinose-inducible *q* (denoted pBAD-*q*)[23]. Q is the phage VP882
120 activator of lytic gene expression. Consequently, the addition of arabinose to the surviving cells
121 induced the lytic program in lysogens, thereby killing those cells. Presumably, this strategy
122 resulted in survival of only *V. parahaemolyticus* 882 mutants resistant to phage VP882 infection
123 (Figure 2A).

124 We screened surviving colonies for phage VP882 genes using PCR to ensure that the isolated
125 mutants were phage-free. All phage-free mutants had acquired a translucent colony morphology
126 that differed from that of the *V. parahaemolyticus* 882 parent, suggesting a modification to the
127 cell surface (Figure S1A). Indeed, phage VP882 could not adsorb to nor form plaques on these
128 mutants (Figure 2B and C, respectively; panel C shows one representative mutant). We sequenced
129 the transposon insertion sites in 19 of these mutants. All of the insertions mapped to the K-
130 antigen/capsule locus (*VP0215-VP0237*)[24] suggesting that this surface polymer could be the
131 phage VP882 receptor (Figure 2D, Table S1). We generated in-frame deletions of *VP0230*
132 (encoding a glycosyltransferase) and *VP0235* (encoding an epimerase) in the *V. parahaemolyticus*
133 882 chromosome and verified by adsorption and plaque assays that the phage could not adsorb

134 nor propagate (Figure 2E and F, respectively), and identical to the original transposon insertion
135 mutants, the deletion strains displayed the translucent colony morphology (Figure S1B; Δ*VP0235*
136 is shown as the example). Some phages can use multiple host receptors to infect. To test whether
137 phage VP882 might have such a capability, we assessed whether lysogenization of the *V.*
138 *parahaemolyticus* Δ*VP0235* mutant occurred after extended incubation with a variant of phage
139 VP882 carrying chloramphenicol resistance (denoted VP882$^{gp38::\mathrm{Cm}}$). *gp38* encodes a phage VP882
140 accessory gene[25] and elimination of it does not affect phage VP882 lysis of host cells (Figure S1C).
141 This approach yielded no chloramphenicol resistant lysogens indicating that the *V.*
142 *parahaemolyticus* K-antigen is the receptor for phage VP882 (Figure S1D).

143 Our identification of the K-antigen as the determinant of phage VP882 infectivity suggested that
144 phage VP882 may specifically infect *V. parahaemolyticus* strains of the O3:K6 serotype, the
145 serotype of its *V. parahaemolyticus* 882 host. To test this possibility, we screened our collection
146 of *V. parahaemolyticus* isolates for susceptibility to phage VP882 infection by plaque assay. While
147 not all of the serotypes of our isolates have been reported, phage VP882 formed plaques
148 exclusively on isolates classified as serotype O3:K6 (Figure 2G and H; we discuss the differences
149 in the extent of plaquing in the next section). Verifying this finding, only *V. parahaemolyticus*
150 O3:K6 isolates produced chloramphenicol resistant colonies following infection with phage
151 VP882$^{gp38::\mathrm{Cm}}$ (Figure S1E).

152 Notably, in the case of one of our O3:K6 serotype isolates, *V. parahaemolyticus* strain VP81, two
153 colony morphologies were present in the stock obtained from ATCC (Figure S1F, designated col1
154 and col2 for colony type 1 and colony type 2). Colony type 1 had an opaque morphology
155 resembling wildtype (WT) *V. parahaemolyticus* 882, and this *V. parahaemolyticus* VP81

156 morphotype was susceptible to phage VP882 infection and underwent lysis. By contrast, colony
157 type 2 was translucent, resembling our *V. parahaemolyticus* 882 K-antigen mutants and was
158 resistant to phage VP882 plaquing (Figure 2H and I). Whole genome sequencing of one colony of
159 each morphotype revealed that the *V. parahaemolyticus* VP81 translucent colony 2 type
160 possesses a frameshift mutation in *VP0235*, a gene in the K-antigen locus and a gene also
161 identified in our transposon mutagenesis. Repair of this point mutation converted the colony
162 from translucent to opaque (Figure S1F) and, moreover, restored the ability of phage VP882 to
163 adsorb and plaque (Figure 2I and H, respectively). Together, our data support the model that the
164 O3:K6 K-antigen is the receptor for phage VP882, and phage VP882 specifically attaches to and
165 infects *V. parahaemolyticus* O3:K6 isolates because of its dependence on this antigen.

166 The particular features of *V. parahaemolyticus* O- and K-antigens that correspond to distinct
167 serotypes have not been defined, so we cannot predict what K6 K-antigen moieties are recognized
168 by phage VP882 nor how its relationship to the O3 O-antigen appendage affects phage VP882
169 recognition. Nonetheless, to preliminarily probe the basis for specificity of phage VP882 host
170 range, we analyzed the O- and K-antigen loci in the genome sequences of our collection of *V.*
171 *parahaemolyticus* strains. In agreement with our observations, all isolates designated O3:K6
172 harbor highly similar O- and K-antigen loci whereas these loci are markedly different in the
173 genomes of non-O3:K6 strains. Few genes encoded in the K-antigen locus of *V. parahaemolyticus*
174 O3:K6 can be identified in the other *V. parahaemolyticus* strains suggesting that their K-antigens
175 are distinct. We conclude that the O3:K6 K-antigen is the essential receptor used by phage VP882.

176 **LuxO-driven quorum sensing controls phage VP882 plaquing**

177 Phage VP882 plaqued on all isolates of *V. parahaemolyticus* O3:K6 possessing genes encoding
178 functional K-antigens. However, the extent of plaquing differed depending on the strain (Figure
179 2H). Specifically, when plated on *V. parahaemolyticus* 882 and *V. parahaemolyticus* VP47, phage
180 VP882 readily formed large plaques at all phage concentrations. By contrast, on *V.*
181 *parahaemolyticus* RIMD and *V. parahaemolyticus* VP81, phage VP882 formed plaques only at the
182 highest concentration tested and the plaques were small. While *V. parahaemolyticus* VP47 and
183 VP81 have not been well studied, one established difference between *V. parahaemolyticus* 882
184 and *V. parahaemolyticus* RIMD concerns their QS systems[20]. *V. parahaemolyticus* 882 harbors an
185 897 base pair deletion that eliminates the *vqmR* promoter, the *vqmR* coding sequence, and a
186 portion of the non-coding region upstream of *vqmA*. Additionally, the *V. parahaemolyticus*
187 882 *luxO* gene (denoted $luxO_{882}$) harbors a 36 bp deletion that causes $LuxO_{882}$ to function as a
188 phospho-mimetic. These mutations lock the respective QS systems into their low cell density
189 modes. Given the connections between host QS and phage VP882 lifestyle transitions, we
190 wondered whether these differences in QS capabilities could influence the differences in phage
191 VP882 plaquing on the various host strains. To probe this possibility, we repaired one or both QS
192 systems in *V. parahaemolyticus* 882 and assessed phage VP882 plaquing (Figure 3A and B).
193 Restoration of VqmA-VqmR QS in *V. parahaemolyticus* 882 (denoted $vqmRA^{+}$) did not affect phage
194 VP882 plaquing ability nor plaque size, and that was irrespective of the status of *luxO*. By contrast,
195 when LuxO was restored to WT function (denoted $luxO^{+}$), phage VP882 made fewer and smaller
196 plaques, similar to its behavior when plated on *V. parahaemolyticus* RIMD that possesses a
197 functional LuxO (Figures 3A and 2H, respectively). Since plaque assays are performed at high cell
198 density, this result indicated that LuxO-directed QS controls the ability of phage VP882 to plaque

199 on *V. parahaemolyticus.* To verify this supposition, we replaced the native *luxO*$_{882}$ with either
200 *luxO*^{D61E} or *luxO*^{D61A} that, respectively, lock *V. parahaemolyticus* into the low cell density and high
201 cell density QS modes. Phage VP882 plaquing on *V. parahaemolyticus* 882 carrying *luxO*^{D61E} was
202 comparable to that on the parent *V. parahaemolyticus* 882 strain that carries the naturally low
203 cell density locked *luxO*^{882} variant. *V. parahaemolyticus* 882 carrying *luxO*^{D61A} displayed phage
204 VP882 plaquing comparable to that on strains with WT *luxO* (Figure 3A and B).

205 The plaquing phenotypes associated with the different *luxO* alleles mirrored the genotypes of the
206 tested *V. parahaemolyticus* O3:K6 isolates. As mentioned, LuxO$_{882}$ locks *V. parahaemolyticus* 882
207 into the low cell density QS state, whereas LuxO in *V. parahaemolyticus* RIMD displays WT
208 function and transitions from the low cell density to the high cell density QS state during growth.
209 LuxO of *V. parahaemolyticus* VP47 harbors an M15R substitution. Analogous to *V.*
210 *parahaemolyticus* 882 and all *V. parahaemolyticus* strains carrying *luxO*^{D61E}, *V. parahaemolyticus*
211 VP47 was incapable of activating a P*luxC* reporter, the canonical QS-activated luciferase promoter
212 that is used as the standard readout for QS function in vibrios[20] (Figure 3C). Thus, *V.*
213 *parahaemolyticus* VP47 is locked in low cell density QS mode. Indeed, changing the arginine at
214 position 15 back to methionine in *V. parahaemolyticus* VP47 LuxO restored density-dependent
215 activation of P*luxC* (Figure 3C). Consistent with this finding, phage VP882 plaques only formed on
216 *V. parahaemolyticus* VP47 carrying the repaired LuxO at high phage concentrations, and the
217 plaques were smaller than those on the parent strain with the *luxO*^{M15R} allele (Figure 3D).
218 Together, our data show that signaling through the LuxO-controlled QS pathway dictates the
219 robustness of phage VP882 plaquing on *V. parahaemolyticus*.

220 ***VPA1602-VPA1604* are quorum-sensing-controlled components that shield *V.***
221 ***parahaemolyticus* from infection by phage VP882**

222 We previously reported that LuxO QS signaling inhibits phage VP882 lysogenization at high cell
223 density in *V. parahaemolyticus* RIMD[23]. Here, we show that a similar phenomenon occurs in *V.*
224 *parahaemolyticus* 882, the natural host for phage VP882: higher numbers of lysogens formed
225 during infection when the host is locked into low cell density QS mode than following infection of
226 the host locked into high cell density QS mode (Figures 3E and S2A). One possibility was that these
227 differences stemmed from differences in the ability of the phage to adsorb to its *V.*
228 *parahaemolyticus* host when the host exists in the low and high cell density locked QS modes.
229 Indeed, 3-fold less phage VP882 adsorption occurred to *V. parahaemolyticus* 882 encoding WT
230 *luxO* and $luxO^{D61A}$ than to *V. parahaemolyticus* 882 harboring the $luxO_{882}$ and $luxO^{D61E}$ alleles
231 (Figures 3F and S2B). These data indicate that a QS-controlled factor influences phage VP882
232 entry into naïve host cells. We considered that QS might control production of the K-antigen.
233 However, examination of RNA-sequencing data from *V. parahaemolyticus* 882 carrying either WT
234 *luxO*, $luxO_{882}$, $luxO^{D61E}$, or $luxO^{D61A}$ showed no significant differences in K-antigen transcript levels
235 (Figure S3A)[20]. Thus, we suspected that some other component regulated by LuxO exists in *V.*
236 *parahaemolyticus* strains and affects phage VP882 adsorption and entry.

237 To identify the putative factor that inhibits phage VP882 entry into *V. parahaemolyticus* 882, we
238 carried out a selection for *V. parahaemolyticus* 882 mutants displaying enhanced phage VP882
239 adsorption and entry at high cell density. Specifically, we generated a transposon mutant library
240 in *V. parahaemolyticus* 882 carrying $luxO^{D61A}$, infected it with phage $VP882^{gp38::Cm}$, and selected
241 chloramphenicol resistant lysogens. Sequencing of the transposon insertion sites in 54 lysogens

242 (Table S2) revealed that nearly all insertions resided in unique locations. Most interesting to us
243 were four insertions in or near the *VPA1602-4* operon. *VPA1602-4* are predicted to encode
244 homologs of Wza, Wzb, and Wzc. Wzabc proteins are involved in export of extracellular
245 polysaccharides such as those required for the *Escherichia coli* Group 1 capsules[26]. Deletion of
246 this operon in *V. parahaemolyticus* strains of the O3:K6 serotype have no effect on K-antigen
247 production[24], so we hypothesized that VPA1602-4 are involved in the production and export of a
248 polysaccharide that blocks access of phage VP882 to the K-antigen. Indeed, deletion of *VPA1602-*
249 *4* restored the ability of phage VP882 to adsorb to *V. parahaemolyticus* 882 *luxO*^{D61A} (Figure 4A).
250 Furthermore, adsorption to all tested *V. parahaemolyticus* 882 strains required the K-antigen
251 including in the absence of *VPA1602-4* (Figure 4A). Consistent with our findings, transcription of
252 *VPA1602-4* is activated at high cell density (Figure S3B and C)[20] and the homologous operon in
253 *Vibrio harveyi* (*VIBHAR_06665-7*) is repressed at low cell density[27]. These patterns, coupled with
254 our data showing that mutation of *VPA1602-4* promotes phage VP882 adsorption to *V.*
255 *parahaemolyticus* 882 *luxO*^{D61A}, suggest that VPA1602-4 are involved in production and export of
256 a polysaccharide that blocks phage access to the K-antigen.

257 The export substrates of VPA1602-4 in *V. parahaemolyticus* are undefined. Table S2 shows that,
258 in the above screen, we also isolated singleton transposon insertions in genes involved in
259 polysaccharide biosynthesis pathways (*galU, nagE,* and *neuC*) that enabled phage VP882 entry.
260 We considered that these additional genes could provide clues concerning the polysaccharide
261 produced by VPA1602-4. However, deletion of these genes had no effect on phage VP882
262 adsorption, so we conclude that they are not required for production of the polysaccharide
263 exported by VPA1602-4 (Figure S3D). We did not investigate the functions of these genes further.

264 Possibly, the VPA1602-4 system exports multiple substrates that affect K-antigen access to phage
265 VP882 explaining why we did not identify the polymer in the transposon screen.

266 Deletion of *VPA1602-4* enabled phage VP882 to adsorb to all *V. parahaemolyticus* 882 hosts
267 irrespective of QS genotype (Figures 3A and S3E). Restoration of phage VP882 adsorption via
268 elimination of *VPA1602-4* also rescued the ability of phage VP882 to lysogenize each *V.*
269 *parahaemolyticus* strain under study to near equivalent levels (Figures 3B and S3F) while having
270 no discernable effect on phage VP882 plaquing (Figure S3G). These results indicate that the major
271 determinant of the LuxO QS effect on phage VP882 lysogenization of *V. parahaemolyticus* 882 is
272 through suppression of phage VP882 virion adsorption to host cells and not via effects on the
273 subsequent lysis-lysogeny decision. Thus, LuxO QS regulation of *VPA1602-4* is a host mechanism
274 that influences the spread of phage VP882 in *V. parahaemolyticus* O3:K6 populations by shielding
275 the K6-antigen (Figure 4C).

276 **Superinfection of *V. parahaemolyticus* phage VP882 lysogens leads to phage VP882 genome**
277 **recombination**

278 The above data define how LuxO QS influences phage VP882 transmission to naïve hosts. An
279 outstanding question remained regarding the fate of phage VP882 virions released into a
280 population of QS *V. parahaemolyticus* O3:K6 cells in which virions are likely to encounter hosts
281 that are already lysogens. Superinfection exclusion, via alteration of the expression or function of
282 the phage receptor, is often employed by lysogens to prevent re-infection[12]. We wondered if
283 phage VP882 encodes a superinfection exclusion mechanism that would prevent it from infecting
284 lysogens.

285 We examined superinfection by plaque assay. Phage VP882 did not form plaques when plated on
286 *V. parahaemolyticus* 882 that was already lysogenic for phage VP882 (Figure 5A). However, in this
287 experiment, homoimmunity, mediated by the resident phage VP882 cI repressor of lysis, could
288 have prevented infecting phages from initiating the lytic replication program necessary for plaque
289 formation even if the virions had adsorbed to and infected lysogens. By exploiting a phage VP882
290 lysogen that cannot produce functional virions, we found that phage VP882 can indeed adsorb to
291 *V. parahaemolyticus* 882 cells that are already lysogenized with phage VP882 (Figure 5B). Thus,
292 no superinfection exclusion mechanism prevents adsorption of phage VP882 virions to
293 lysogenized hosts.

294 Following adsorption to *V. parahaemolyticus* 882 lysogens, we wondered whether injection of
295 the phage genome occurred. To probe this issue, we assessed whether infection of *V.*
296 *parahaemolyticus* 882 lysogens with phage VP882$^{gp38::\mathrm{Cm}}$ generated chloramphenicol resistant
297 colonies. Indeed, chloramphenicol resistant lysogens were produced at levels similar to those
298 resulting from infection of *V. parahaemolyticus* 882 that had been cured of phage VP882 (Figure
299 5C). Thus, phage VP882 virions can both attach to lysogenic cells and inject their genomes. We
300 call new lysogens, which originate from existing *V. parahaemolyticus* 882 phage VP882 lysogens
301 and acquire DNA from an infecting phage VP882, superlysogens.

302 The influence of QS on phage VP882 lysogenization of *V. parahaemolyticus* 882 via regulation of
303 *VPA1602-4* was maintained during superinfection. Specifically, lysogens of *V. parahaemolyticus*
304 882, which is naturally locked into the low cell density QS mode, were converted to
305 chloramphenicol resistant superlysogens at a higher frequency than were *V. parahaemolyticus*
306 882 lysogens locked into high cell density QS mode (Figure 5C). Deletion of *VPA1602-4* restored

307 lysogenization of both the phage-cured and lysogenized high cell density locked QS *V.*
308 *parahaemolyticus* 882 strains to the levels of the corresponding *V. parahaemolyticus* 882 low cell
309 density locked cured and lysogenic strains (Figure 5C). These results indicate that LuxO regulation
310 of *VPA1602-4* occurs in *V. parahaemolyticus* 882 lysogens and non-lysogens, and thus, host QS
311 status dictates the outcome of phage VP882 superinfection by affecting phage entry.

312 The transfer of chloramphenicol resistance following phage VP882$^{gp38::\mathrm{Cm}}$ infection of *V.*
313 *parahaemolyticus* 882 lysogens indicates that lysogens acquire superinfecting phage DNA. We
314 considered the fates of the resident and superinfecting phage genomes during phage VP882
315 superinfection and superlysogenization. Phage VP882 is a linear plasmid-phage that exists in
316 multiple copies per cell. Superinfection could result in a heterogeneous population of phage
317 genomes. Alternatively, superinfection could result in exchange of the existing phage genomes
318 with the infecting phage genome. Finally, superinfection could result in recombination of resident
319 and infecting phage genomes. To test which possibility occurs, we infected *V. parahaemolyticus*
320 882 lysogens with phage VP882 harboring a chloramphenicol marker in an intergenic region near
321 the 3' terminus of the phage genome (denoted VP882$^{gp71\text{-intergenic::Cm}}$). We investigated whether
322 the chloramphenicol resistance marker was maintained in lysogens that acquired gentamicin
323 resistance during superinfection with phage VP882 carrying a gentamicin resistance marker in
324 *gp38* (denoted VP882$^{gp38::\mathrm{Gm}}$). *gp38* is located near the center of the phage genome (Figure S4).
325 We reasoned that if the phage genomes co-exist following superinfection, all superlysogens
326 would be both gentamicin and chloramphenicol resistant. By contrast, if the phage genomes were
327 exchanged, all superlysogens would exhibit only gentamicin resistance. Third and lastly, if
328 recombination of phage genomes occurred, some superlysogens would be exclusively gentamicin

329 resistant and some would display resistance to both gentamicin and chloramphenicol.
330 Importantly, our method only allows us to detect superlysogenization events that result in the
331 acquisition of gentamicin resistance, we cannot detect events in which gentamicin is acquired
332 and then lost following recombination (Figure S4). The third possibility occurred (Figure 5D)
333 suggesting that recombination occurs between the resident and newly infecting phage genomes.
334 Deletion of *recA*, encoding the recombinase required to initiate homologous recombination, did
335 not affect the level of lysogenization of naïve *V. parahaemolyticus* 882 nor of *V. parahaemolyticus*
336 882 lysogenized with phage VP882 (Figure 5E). However, *V. parahaemolyticus* 882 Δ*recA* lysogens
337 carrying VP882$^{gp71\text{-intergenic::Cm}}$ did not yield doubly antibiotic-resistant superlysogens when
338 infected with phage VP882$^{gp38\text{::Gm}}$ (Figure 5D); all of the colonies that had acquired gentamicin
339 resistance had lost chloramphenicol resistance. Furthermore, infection of *V. parahaemolyticus*
340 882 lysogens carrying VP882$^{gp38\text{::Cm}}$ with phage VP882$^{gp38\text{::Gm}}$ did not yield doubly antibiotic-
341 resistant lysogens (Figure 5D). Thus, when recombination that places both antibiotic resistance
342 markers onto the same phage genome is prevented or is not possible, the superlysogens acquire
343 the entire genome of the infecting phage. Together, these results suggest that only one variant of
344 the phage VP882 genome is maintained in *V. parahaemolyticus* and, during superinfection,
345 recombination occurs between the infecting and resident phage genomes to enable this
346 outcome.

347 To confirm the above findings, we tested whether all the phage genomes in a *V. parahaemolyticus*
348 882 superlysogen were identical or not. To do this, we used PCR amplification of the loci
349 containing the resistance cassettes in doubly-antibiotic resistant *V. parahaemolyticus* 882
350 superlysogens (Figure S4). The logic is if only one phage genome is present, PCR amplification

351 spanning either the *gp38* or the *gp71*-intergenic locus will yield a single PCR product, while if two
352 phage genomes are maintained, PCR amplification should yield two PCR products corresponding
353 to the allele containing and lacking the resistance marker. PCR amplification yielded one product
354 for each locus, and the product size corresponded to the phage with the resistance cassette in
355 each locus (Figure 5F). Additionally, both gentamicin and chloramphenicol resistance were
356 maintained when these superlysogens were grown in the absence of antibiotic selection. This
357 result indicated that the markers were linked and could not independently segregate over
358 multiple generations. These data support our model that recombination occurs between the
359 infecting and resident phage genomes during superinfection and only one variant of the phage
360 genome is maintained.

361 **Discussion**

362 Phage VP882 engages with both QS systems of its host *V. parahaemolyticus* and funnels the
363 information it garners into control of transitions between lysogeny and lytic replication (Figure 1).
364 Monitoring host QS enables phage VP882 to favor transitioning from lysogeny to lysis at high host
365 cell densities. Presumably, skewing transitions in this direction increases the frequency of
366 released phage VP882 virions encountering new host cells. An outstanding question was whether
367 those encounters are productive given that monitoring host QS cues does not provide the phage
368 information concerning whether or not nearby host cells are already lysogens. Irrespective of
369 encounter frequency, populations of hosts that are predominantly lysogens could restrict phage
370 VP882 transmission if resident VP882 phages deploy homoimmunity or superinfection exclusion
371 mechanisms that block subsequent phage infection or propagation.

372

373 Here, we identify and characterize host components that influence transmission of phage VP882
374 in QS populations of *V. parahaemolyticus*. We identify the receptor used by phage VP882 as the
375 O3:K6 K-antigen that is specific to its host strain (Figure 2B-F). We show that phage access to the
376 O3:K6 K-antigen is controlled by LuxO-driven QS regulation of a transport system that exports
377 polysaccharides that shield the K-antigen from the phage at high cell density (Figure 4A and C).
378 We demonstrate that phage VP882 does not encode a superinfection exclusion mechanism, so *V.*
379 *parahaemolyticus* lysogens can be superinfected by virions released from neighboring cells
380 (Figure 5D). Our data demonstrate that following superinfection, DNA from newly infecting phage
381 genomes can be maintained in the entirety or can recombine with the resident phage genome
382 resulting in superlysogenic conversion (Figure 5D and F). Thus, phage VP882 avoids unproductive
383 encounters with already lysogenized hosts. We propose that, together, superinfection and phage
384 genome recombination promote phage VP882 spread and genomic diversity in lysogenic *V.*
385 *parahaemolyticus* populations.
386
387 Phage VP882 could employ the specific K-antigen receptor to ensure transmission to similar hosts
388 to which the phage arrives well-adapted. As a plasmid-phage, and we have experimentally
389 demonstrated this trait previously[6], phage VP882 can persist in, replicate in, and lyse a wide
390 variety of very distantly related/unrelated bacterial species because its RepA module is sufficient
391 for plasmid maintenance and does not require a specific site in the host genome for the phage to
392 lysogenize. However, the narrow distribution of the O3:K6 receptor guarantees that, in natural
393 settings, phage VP882 exclusively infects *V. parahaemolyticus* strains of that serotype.
394 Interestingly, both the LuxO and VqmR-VqmA systems that influence phage VP882 lifestyle

395 transitions are only present in *vibrio spp*[5,6]. Rigid receptor-specificity could serve as a gate-keeping
396 mechanism to ensure the prophage receives the benefits of detecting and responding to the
397 multiple host QS signals by restricting infection to only similar *V. parahaemolyticus* strains.
398 Recently, VP882-like plasmid-phages have been discovered that reside in other bacterial
399 species[25]. It will be fascinating to learn if they too use specific receptors that constrain host range
400 to hosts to which they are likewise highly adapted.
401
402 While QS plays an overarching role in interactions between phage VP882 and its *V.*
403 *parahaemolyticus* host, here, we find that QS also drives host adaptation to the phage.
404 Specifically, at high cell density, LuxO-QS activates production of a polysaccharide export system
405 that protects *V. parahaemolyticus* from phage VP882 adsorption and therefore, infection. In other
406 phage-bacterial systems, QS-controlled restriction of phage propagation is mediated by
407 alterations in phage receptor availability, via upregulation of CRISPR systems, and through control
408 of abortive infection mechanisms[28–31]. In the current case, we find that changes in phage VP882
409 adsorption do not alter phage VP882 lytic propagation but, rather, affect the ability of phage
410 VP882 to lysogenize its host. Clearly, additional QS-controlled mechanisms that modulate phage
411 VP882 activity exist in *V. parahaemolyticus* that, for example, contribute to differences in phage
412 VP882 plaquing when phage VP882 adsorption is equivalent among strains (Figure S3G).
413 Potentially, *V. parahaemolyticus* has evolved multiple strategies to counteract phage VP882 in
414 response to the phage's pervasive infective capability.
415

416 Rather than deploying a superinfection exclusion mechanism that diverts phage VP882 progeny
417 to infection of naïve hosts[12] or a mechanism that detects the abundance of lysogens or like phages
418 in the vicinal community[3], phage VP882 infects lysogens that already harbor phage VP882. While
419 phage VP882 does not propagate immediately following superinfection, as noted above, these
420 infection events are not unproductive, as the newly infecting phage DNA can be maintained in
421 the superinfected host. We propose that coupling surveillance of QS cues with superinfection is
422 especially beneficial to phage VP882 compared to phages that do not possess one or both of
423 these capabilities. First, lysis primarily occurs when many potential host cells are present and
424 infection or superinfection promotes phage transmission. Second, superlysogenization could
425 promote phage VP882 genetic diversity. Our data indicate that the primary outcome of
426 superlysogenization is that a single phage genome is maintained in the host. Consistent with our
427 notion that this process fosters genomic diversity, we demonstrate that, in many cases,
428 superinfection results in recombination between the resident and infecting phage genomes. We
429 detect these events in 1-5% of superlysogens (Figure 5D), but the frequency of recombination is
430 likely higher as only a subset of recombination events can be detected by our markers.
431 Superinfection resulting in either genome exchange or recombination potentially enhances the
432 spread of phage VP882 variants because genomes of variants with reduced fitness can be
433 replaced by genomes or portions of genomes from successfully replicating and successfully
434 superinfecting phages. The narrow host specificity phage VP882 displays via dependence on the
435 K6 antigen presumably increases the likelihood that, if virions encounter a lysogen that the virion
436 can infect, the resident phage genome will be similar enough to the newly infecting phage
437 genome for recombination to occur.

438

439 Together, our data reveal that phage VP882 transmission is influenced by both host and phage
440 features that hinge on bacterial QS inputs. At high host cell density, phage VP882 lytic replication
441 is stimulated by inputs from both QS systems of *V. parahaemolyticus* host cells[6,20]. Superinfection
442 enables phage VP882 to overcome the challenge temperate phages face when they induce their
443 lytic cycle in populations of lysogens. In this case, superinfection moreover ensures that phage
444 VP882 can capitalize on its interception of bacterial QS cues. *V. parahaemolyticus* host cells "fight
445 back" by restricting phage VP882 spread using QS-directed production of a receptor-shielding
446 molecule, also at high cell density. Potentially, this host strategy could broadly defend against
447 phage infection. In the context of our current work, the receptor-shielding mechanism tips phage
448 VP882 lysogeny toward naïve host populations and conditions of low host abundance, both of
449 which are non-optimal for phage VP882 to propagate and diversify. Thus, bacterial QS signaling
450 underlies both host and phage behaviors that shape the outcomes of phage VP882 replication
451 and host encounters. These dynamics could differ for other phage-host pairs depending on the
452 selection pressures germane to their specific environments and the mechanisms connecting
453 phage processes to host QS signaling.

454

455

456 **Materials and Methods**

457 **Bacterial strains, reagents, and growth conditions**

458 *Escherichia coli* strains were grown with aeration in Lysogeny Broth (LB-Miller, BD-Difco) at 37
459 °C. *V. parahaemolyticus* strains were grown with aeration in LM (LB with 2% NaCl) at 30 °C. Strains
460 used in the study are listed in Table S3. Unless otherwise noted, antibiotics were used at: 50
461 µg/mL kanamycin (GoldBio), 50 µg/mL polymyxin B (Sigma), 10 µg/mL chloramphenicol (Sigma),
462 and 30 µg/mL gentamicin (Sigma). Diaminopimelic acid (DAP, Sigma) was used at 100 µM. For
463 phage lysis and bioluminescent reporter assays, overnight cultures of *V. parahaemolyticus* strains
464 were diluted 1:100 into fresh LM containing antibiotics when appropriate. After 2 h of growth at
465 30 °C with aeration, cultures were diluted 1:100 into fresh medium with appropriate antibiotics
466 prior to being dispensed (200 µL/well) into 96 well plates (Corning Costar 3903). When needed,
467 0.05 µg/mL mitomycin C was added at the second dilution step. A BioTek Synergy Neo2 Multi-
468 Mode reader was used to measure OD_{600} and bioluminescence. Relative Light Units (RLU) are
469 bioluminescence divided by OD_{600}. P*luxC-luxCDABE* expression was measured at 300 min of
470 growth. P*VPA1602-luxCDABE* expression was measured at 500 min of growth.

471

472 **Cloning techniques**

473 All primers used for plasmid construction and qPCR, listed in Table S4, were obtained from
474 Integrated DNA Technologies. FastCloning[32]or Gibson Assembly (NEB) were employed for plasmid
475 assembly. Briefly, PCR was performed with Q5 polymerase (NEB) to generate cloning inserts. In
476 the case of pTOX2[33], linear plasmid backbone was generated by restriction digestion with SwaI
477 (NEB). Inserts in assembled plasmids were verified by sequencing (Azenta Genewiz or

478 Plasmidsuarus). Plasmids used in this study are listed in Table S5. Transfer of plasmids into
479 *V. parahaemolyticus* was accomplished by conjugation with *E. coli* S17 or MFD*pir*[34] (a DAP
480 auxotroph) followed by selective plating on LB plates containing appropriate antibiotics. Mutants
481 were generated by allelic exchange with 15% sucrose (pRE112 backbone) or 2% rhamnose (pTOX2
482 backbone) for counter selection. Mutations were verified by colony PCR or Sanger sequencing. To
483 insert antibiotic cassettes into the phage VP882 genome, PCR products containing the antibiotic
484 cassette flanked by homologous phage VP882 DNA sequences were introduced by natural
485 transformation. Competence of *V. parahaemolyticus* 882 was induced by expression of *tfoX*[35].
486 Phages carrying antibiotic cassettes were isolated by lysogenization of *V. parahaemolyticus* 882
487 that had previously been cured of phage VP882.
488
489 **Generation of phage lysates**
490 Overnight cultures of *V. parahaemolyticus* 882 strains lysogenized with phage VP882 were diluted
491 1:100 in LM and incubated for 2 h at 30 °C with aeration (180 rpm). Mitomycin C was added and
492 growth continued for 2.5 h. Lysates of lytic phage VP882 were generated by infection of *V.*
493 *parahaemolyticus* 882 that had been cured of phage VP882 for 16 h at 30 °C with aeration. Debris
494 was removed from lysed cultures by centrifugation (10,000 x g for 1 min). Clarified supernatant
495 was treated with 0.5 % chloroform for at least 15 min prior to use. Phage lysate titers were
496 quantified by plaque assay.
497
498 **Phage VP882 plaque assay**

499 Phage VP882 plaquing on *V. parahaemolyticus* strains was quantified by the double-layer overlay
500 plaque method[36]. *V. parahaemolyticus* was grown from a single colony to stationary phase (16 h).
501 The culture was diluted 1:100 into molten 0.5% LB agar containing 10 mM $CaCl_2$. The mixture was
502 poured over 1.5% LB agar in a petri plate and allowed to solidify at room temperature for 10-15
503 min. 0.1% Evan's Blue (Sigma) and 0.2% uranine (Sigma) were incorporated into the bottom agar
504 to enhance plaque visibility. 10-fold serial dilutions of phage VP882 lysate (initial titer 10^{-8}-10^{-9}
505 PFU/mL) were spotted onto the plate (3.5 µL/spot) and allowed to dry prior to incubation
506 overnight at 37 °C. Plaques were imaged with an IQ800 imager (Cytvia) using the UV setting and
507 black tray with 0.1 s exposure. Because phage VP882 does not form individual plaques on *V.*
508 *parahaemolyticus* in high cell density QS mode, plaquing was assessed based on clearance and
509 the sizes of plaques as described previously[37]. The lowest 10-fold dilution spot in which clearance
510 occurred was recorded. The log differences in plaquing shown in Figures 3A and S2A are the
511 differences between the plaquing score for the parent *V. parahaemolyticus* 882 strain cured of
512 phage VP882 and the designated strain.
513
514 **Phage VP882 adsorption assay**
515 *V. parahaemolyticus* was grown from a single colony to stationary phase (16 h). The culture was
516 adjusted to OD_{600} 2.5 with LB. 50 µL of this culture was combined with 150 µL of a suspension
517 containing 10 mM $CaCl_2$ and lysate from a spontaneously occurring lytic phage VP882 variant
518 (final MOI 10^{-3}-10^{-4}). The mixture was incubated at room temperature for 20 min. Cells and
519 adsorbed phage particles were separated from free phage by centrifugation (10,000 x g for 1 min).
520 30 µL of the free phage solution was added to 4 mL of 0.5% LB agar containing 10 mM $CaCl_2$ and

521 a 1:100 dilution of a stationary phase culture of *V. parahaemolyticus* 882 that had been cured of
522 phage VP882. The mixture was poured into 3 cm petri dishes (Falcon). Plaques were quantified
523 after overnight incubation at 37 °C. The fraction of unadsorbed phage (% free phage) was
524 calculated by comparing the number of phage to that in an identically treated sample lacking
525 bacteria.
526
527 **Phage VP882 lysogenization assay**
528 *V. parahaemolyticus* was grown from a single colony to stationary phase (16 h). The culture was
529 adjusted to OD_{600} 2.5 with LB. The cell suspension was mixed at a 1:4 ratio with a suspension
530 containing LB, 10 mM $CaCl_2$, and lysate from phage VP882 marked with an antibiotic cassette at
531 an MOI 10^{-5}-10^{-6}. The mixture was incubated without shaking at 30 °C for 1 h prior to plating on
532 nonselective medium to quantify total cells and on selective medium to quantify lysogens. For
533 experiments to test lysogenization of *V. parahaemolyticus* lacking the O3:K6 K-antigen receptor,
534 the entire lysogenization mixture was diluted into 3 mL of fresh LM containing 10 mM $CaCl_2$ and
535 grown for 16 h at 30 °C with aeration before plating on selective medium. Plates were incubated
536 at 37 °C for 16-20 h and colonies counted. Percent lysogens is the number of colonies on selective
537 medium divided by the number on nonselective medium. In all lysogenization quantitation
538 experiments except those examining phage recombination, phage VP882$^{gp38::\mathrm{Cm}}$ was used. In
539 experiments examining phage recombination, lysogens harboring phage VP882$^{gp71\text{-intergenic::Cm}}$
540 were infected with phage VP882$^{gp38::\mathrm{Gm}}$ lysate. Lysogens resistant to both gentamicin and
541 chloramphenicol were isolated and purified to verify dual-resistance. Homogeneity of each locus
542 was assessed by colony PCR with DreamTaq Polymerase (Thermo). PCR products were analyzed

543 on 1% agarose 1X TAE gels stained with SYBR Safe (Edvotek) and imaged with an IQ800 imager
544 (Cytvia) using the Cy2 setting and black tray with auto-exposure.
545
546 **Construction of transposon mutant libraries**
547 Transposon insertion libraries in *V. parahaemolyticus* 882 or *V. parahaemolyticus* 882 *luxO*^{D61A}
548 both of which had been cured of phage VP882 were generated with the Mariner transposon on
549 pSC189 using kanamycin selection[38]. *E. coli* MFD*pir*/pSC189 was used as the donor to deliver
550 pSC189 by conjugation. 300 µL of donor and 100 µL of recipient were mixed. The suspension was
551 subjected to centrifugation (8,000 x g for 2 min) and 390 µL of the clarified culture fluid was
552 removed. Cells were resuspended in the residual medium and spotted on 0.45 µm mixed cellulose
553 ester membrane filters (Millipore) that had been placed onto LB agar plates followed by
554 incubation at 37 °C for 2 h. The filters were transferred to microcentrifuge tubes containing 1 mL
555 of PBS and subjected to vortex to dislodge cells. Various dilutions of the cell suspensions were
556 plated on nonselective and selective media to quantify the number of exconjugants. 10 separate
557 matings were performed to generate the library. Each mating yielded ~35,000-70,000
558 exconjugants. Nested arbitrary PCR (Neo-F + Arb 1, pSC189-1st-3rd + Arb2)[39] was used to assess
559 randomness of transposition. Exconjugants were collected from the plates by scraping all colonies
560 into LB broth containing appropriate antibiotics, resulting in cell suspensions of OD_{600} of ~50.
561 Aliquots of the library were frozen in 30% glycerol.
562
563 **Transposon mutagenesis screen to identify genes encoding the phage VP882 receptor**

564 pBAD-*q* was introduced into the phage-cured *V. parahaemolyticus* 882 transposon mutants from
565 the above library by conjugation. Exconjugants were selected on LB agar containing
566 chloramphenicol and kanamycin. Selection of survivors of phage VP882 infection was performed
567 by diluting the library of mutants containing pBAD-*q* 1:2,000 or 1:20,000 into 8 separate 10 mL
568 aliquots of LB containing 10 mM $CaCl_2$ and phage VP882 to yield 8 different ratios of phage:
569 bacteria at MOI 0.001-2 followed by incubation for 16 h. The infected cultures were back-diluted
570 1:150 into LB broth and grown for 2.5 h at 30 °C with aeration. Subsequently, 0.2% arabinose was
571 added to induce expression of *q* and the cultures grown for 2 h at 30 °C with aeration before
572 plating. Colonies were screened for phage VP882 by PCR for $vqmA_{Phage}$ (primers oMRS1 + oMRS2).
573 All opaque colonies were positive for phage VP882 indicating that they were lysogens (see main
574 text). Phage-free colonies were isolated, and the transposon insertion sites were identified by
575 arbitrary PCR and Sanger sequencing with the pSC189-1st-3rd primer.
576
577 **Transposon mutagenesis screen to identify genes encoding factors that prevent phage VP882**
578 **infection of *V. parahaemolyticus* 882 at high cell density**
579 A thawed aliquot of the *V. parahaemolyticus* 882 $luxO^{D61A}$ transposon mutant library was diluted
580 1:1,000 in 20 mL of LB broth and incubated for 30 min at 30 °C with aeration for resuscitation.
581 The suspension was diluted into 10 tubes containing 10 mM $CaCl_2$ and phage VP882$^{gp38::Cm}$ at MOI
582 10^{-5}-10^{-6}, incubated for 3 h with aeration and then plated on LB + chloramphenicol + kanamycin
583 to select lysogens. Plates were incubated for 20 h at 37 °C and then at room temperature for an
584 additional 24 h. Chloramphenicol-resistant colonies were isolated and transposon insertion sites
585 were identified by arbitrary PCR and Sanger sequencing with the pSC189-1st-3rd primer.

586

587 **Quantitation and statistical analyses**

588 Software used to collect and analyze data generated in this study consisted of: GraphPad Prism
589 10 for visualization of data, calculation of statistics, and analysis of growth and reporter-based
590 experiments; Gen5 for collection of growth and reporter-based data; Geneious v2026.0 for
591 primer design and sequencing verification; Amersham ImageQuant for imaging of plaque assays
592 and agarose gels. Data are presented as the means ± SEMs. Numbers of technical and
593 independent biological replicates are indicated in the figure legends.

Acknowledgements

We are grateful to members of the Bassler laboratory for insightful discussions.

Funding

This material is based upon work supported by the Howard Hughes Medical Institute and the National Science Foundation (grant MCB-2508324) (B.L.B.). The funders had no role in study design, data collection and analysis, decision to publish, or preparation of the manuscript. Any opinions findings and conclusions or recommendations expressed in this material are those of the authors and do not necessarily reflect the views of the National Science Foundation.

Author Contributions

Outlined the study: M.R.S and B.L.B.

Performed experiments: M.R.S

Analyzed data: M.R.S and B.L.B.

Interpreted data: M.R.S and B.L.B.

Wrote manuscript: M.R.S and B.L.B.

Declaration of Interests

The authors declare no competing interests.

Data and code availability

615 No sequencing or custom code is included in this manuscript. All plasmids and strains in this study

616 are available from the corresponding author upon request. All data is available upon request.

617 **References**

618 1. Howard-Varona, C., Hargreaves, K.R., Abedon, S.T., and Sullivan, M.B. (2017). Lysogeny in
619 nature: mechanisms, impact and ecology of temperate phages. ISME J. *11*, 1511–1520.
620 https://doi.org/10.1038/ismej.2017.16.

621 2. Cheong, K.H., Wen, T., Benler, S., Koh, J.M., and Koonin, E.V. (2022). Alternating lysis and
622 lysogeny is a winning strategy in bacteriophages due to Parrondo's paradox. Proc. Natl. Acad.
623 Sci. *119*, e2115145119. https://doi.org/10.1073/pnas.2115145119.

624 3. Erez, Z., Steinberger-Levy, I., Shamir, M., Doron, S., Stokar-Avihail, A., Peleg, Y., Melamed, S.,
625 Leavitt, A., Savidor, A., Albeck, S., et al. (2017). Communication between viruses guides lysis–
626 lysogeny decisions. Nature *541*, 488–493. https://doi.org/10.1038/nature21049.

627 4. Li, G., Cortez, M.H., Dushoff, J., and Weitz, J.S. (2020). When to be temperate: on the fitness
628 benefits of lysis vs. lysogeny. Virus Evol. *6*, veaa042. https://doi.org/10.1093/ve/veaa042.

629 5. Papenfort, K., and Bassler, B.L. (2016). Quorum sensing signal-response systems in Gram-
630 negative bacteria. Nat. Rev. Microbiol. *14*, 576–588.
631 https://doi.org/10.1038/nrmicro.2016.89.

632 6. Silpe, J.E., and Bassler, B.L. (2019). A host-produced quorum-sensing autoinducer controls a
633 phage lysis-lysogeny decision. Cell *176*, 268-280.e13.
634 https://doi.org/10.1016/j.cell.2018.10.059.

635 7. Silpe, J.E., Duddy, O.P., and Bassler, B.L. (2022). Natural and synthetic inhibitors of a phage-
636 encoded quorum-sensing receptor affect phage–host dynamics in mixed bacterial
637 communities. Proc. Natl. Acad. Sci. *119*, e2217813119.
638 https://doi.org/10.1073/pnas.2217813119.

639 8. Kaiser, A.D., and Jacob, F. (1957). Recombination between related temperate bacteriophages
640 and the genetic control of immunity and prophage localization. Virology *4*, 509–521.
641 https://doi.org/10.1016/0042-6822(57)90083-1.
642 9. Brown, S., Mitarai, N., and Sneppen, K. (2022). Protection of bacteriophage-sensitive
643 Escherichia coli by lysogens. Proc. Natl. Acad. Sci. U. S. A. *119*, e2106005119.
644 https://doi.org/10.1073/pnas.2106005119.
645 10. Łoś, J., Zielińska, S., Krajewska, A., Michalina, Z., Małachowska, A., Kwaśnicka, K., and Łoś, M.
646 (2021). Temperate Phages, Prophages, and Lysogeny. In Bacteriophages, D. R. Harper, S. T.
647 Abedon, B. H. Burrowes, and M. L. McConville, eds. (Springer International Publishing), pp.
648 119–150. https://doi.org/10.1007/978-3-319-41986-2_3.
649 11. Bondy-Denomy, J., Qian, J., Westra, E.R., Buckling, A., Guttman, D.S., Davidson, A.R., and
650 Maxwell, K.L. (2016). Prophages mediate defense against phage infection through diverse
651 mechanisms. ISME J. *10*, 2854–2866. https://doi.org/10.1038/ismej.2016.79.
652 12. Bucher, M.J., and Czyż, D.M. (2024). Phage against the machine: the SIE-ence of
653 superinfection exclusion. Viruses *16*, 1348. https://doi.org/10.3390/v16091348.
654 13. Wright, A. (1971). Mechanism of conversion of the *Salmonella* O antigen by bacteriophage
655 ε^{34}. J. Bacteriol. *105*, 927–936. https://doi.org/10.1128/jb.105.3.927-936.1971.
656 14. Uc-Mass, A., Loeza, E.J., De La Garza, M., Guarneros, G., Hernández-Sánchez, J., and
657 Kameyama, L. (2004). An orthologue of the cor gene is involved in the exclusion of temperate
658 lambdoid phages. Evidence that Cor inactivates FhuA receptor functions. Virology *329*, 425–
659 433. https://doi.org/10.1016/j.virol.2004.09.005.

660 15. Broadbent, S.E., Davies, M.R., and Van Der Woude, M.W. (2010). Phase variation controls
661 expression of *Salmonella* lipopolysaccharide modification genes by a DNA methylation-
662 dependent mechanism. Mol. Microbiol. *77*, 337–353. https://doi.org/10.1111/j.1365-
663 2958.2010.07203.x.
664 16. Leavitt, J.C., Woodbury, B.M., Gilcrease, E.B., Bridges, C.M., Teschke, C.M., and Casjens, S.R.
665 (2024). Bacteriophage P22 SieA-mediated superinfection exclusion. mBio *15*, e02169-23.
666 https://doi.org/10.1128/mbio.02169-23.
667 17. Taylor, V.L., Patel, P.H., Shah, M., Yusuf, A., Burk, C.M., Sztanko, K.M., Gitai, Z., Davidson, A.R.,
668 Koch, M.D., and Maxwell, K.L. (2025). Prophages block cell surface receptors to preserve their
669 viral progeny. Nature *644*, 1049–1057. https://doi.org/10.1038/s41586-025-09260-z.
670 18. Papenfort, K., Silpe, J.E., Schramma, K.R., Cong, J.-P., Seyedsayamdost, M.R., and Bassler, B.L.
671 (2017). A *Vibrio cholerae* autoinducer-receptor pair that controls biofilm formation. Nat.
672 Chem. Biol. *13*, 551–557. https://doi.org/10.1038/nchembio.2336.
673 19. Papenfort, K., Förstner, K.U., Cong, J.-P., Sharma, C.M., and Bassler, B.L. (2015). Differential
674 RNA-seq of *Vibrio cholerae* identifies the VqmR small RNA as a regulator of biofilm formation.
675 Proc. Natl. Acad. Sci. *112*. https://doi.org/10.1073/pnas.1500203112.
676 20. Duddy, O.P., Silpe, J.E., Fei, C., and Bassler, B.L. (2023). Natural silencing of quorum-sensing
677 activity protects *Vibrio parahaemolyticus* from lysis by an autoinducer-detecting phage. PLoS
678 Genet. *19*, e1010809. https://doi.org/10.1371/journal.pgen.1010809.
679 21. Huang, X., Duddy, O.P., Silpe, J.E., Paczkowski, J.E., Cong, J., Henke, B.R., and Bassler, B.L.
680 (2020). Mechanism underlying autoinducer recognition in the *Vibrio cholerae* DPO-VqmA

681 quorum-sensing pathway. J. Biol. Chem. *295*, 2916–2931.
682 https://doi.org/10.1074/jbc.RA119.012104.
683 22. Silpe, J.E., Bridges, A.A., Huang, X., Coronado, D.R., Duddy, O.P., and Bassler, B.L. (2020).
684 Separating functions of the phage-encoded quorum-sensing-activated antirepressor Qtip.
685 Cell Host Microbe *27*, 629-641.e4. https://doi.org/10.1016/j.chom.2020.01.024.
686 23. Santoriello, F.J., and Bassler, B.L. (2024). The LuxO-OpaR quorum-sensing cascade
687 differentially controls Vibriophage VP882 lysis-lysogeny decision making in liquid and on
688 surfaces. PLOS Genet. *20*, e1011243. https://doi.org/10.1371/journal.pgen.1011243.
689 24. Chen, Y., Dai, J., Morris, J.G., and Johnson, J.A. (2010). Genetic analysis of the capsule
690 polysaccharide (K antigen) and exopolysaccharide genes in pandemic Vibrio
691 parahaemolyticus O3:K6. BMC Microbiol. *10*, 274. https://doi.org/10.1186/1471-2180-10-
692 274.
693 25. Santoriello, F.J., and Bassler, B.L. (2026). A family of linear plasmid phages that detect a
694 quorum-sensing autoinducer exists in multiple bacterial species. mBio *17*, e02320-25.
695 https://doi.org/10.1128/mbio.02320-25.
696 26. Whitfield, C. (2009). Structure and assembly of *Escherichia coli* capsules. EcoSal Plus *3*,
697 10.1128/ecosalplus.4.7.3. https://doi.org/10.1128/ecosalplus.4.7.3.
698 27. Shao, Y., Feng, L., Rutherford, S.T., Papenfort, K., and Bassler, B.L. (2013). Functional
699 determinants of the quorum-sensing non-coding RNAs and their roles in target regulation.
700 EMBO J. *32*, 2158–2171. https://doi.org/10.1038/emboj.2013.155.

701 28. Høyland-Kroghsbo, N.M., Mærkedahl, R.B., and Svenningsen, S.L. (2013). A quorum-sensing-
702 induced bacteriophage defense mechanism. mBio *4*, e00362-12.
703 https://doi.org/10.1128/mBio.00362-12.
704 29. Tan, D., Svenningsen, S.L., and Middelboe, M. (2015). Quorum sensing determines the choice
705 of antiphage defense strategy in vibrio anguillarum. mBio *6*, e00627.
706 https://doi.org/10.1128/mBio.00627-15.
707 30. Patterson, A.G., Jackson, S.A., Taylor, C., Evans, G.B., Salmond, G.P.C., Przybilski, R., Staals,
708 R.H.J., and Fineran, P.C. (2016). Quorum sensing controls adaptive immunity through the
709 regulation of multiple CRISPR-Cas systems. Mol. Cell *64*, 1102–1108.
710 https://doi.org/10.1016/j.molcel.2016.11.012.
711 31. Høyland-Kroghsbo, N.M., Paczkowski, J., Mukherjee, S., Broniewski, J., Westra, E., Bondy-
712 Denomy, J., and Bassler, B.L. (2017). Quorum sensing controls the *Pseudomonas aeruginosa*
713 CRISPR-Cas adaptive immune system. Proc. Natl. Acad. Sci. *114*, 131–135.
714 https://doi.org/10.1073/pnas.1617415113.
715 32. Li, C., Wen, A., Shen, B., Lu, J., Huang, Y., and Chang, Y. (2011). FastCloning: a highly simplified,
716 purification-free, sequence- and ligation-independent PCR cloning method. BMC Biotechnol.
717 *11*, 92. https://doi.org/10.1186/1472-6750-11-92.
718 33. Lazarus, J.E., Warr, A.R., Kuehl, C.J., Giorgio, R.T., Davis, B.M., and Waldor, M.K. (2019). A new
719 suite of allelic-exchange vectors for the scarless modification of proteobacterial genomes.
720 Appl. Environ. Microbiol. *85*, e00990-19. https://doi.org/10.1128/AEM.00990-19.
721 34. Ferrières, L., Hémery, G., Nham, T., Guérout, A.-M., Mazel, D., Beloin, C., and Ghigo, J.-M.
722 (2010). Silent mischief: Bacteriophage Mu insertions contaminate products of <Escherichia

723 coli</i> random mutagenesis performed using suicidal transposon delivery plasmids
724 mobilized by broad-host-range RP4 conjugative machinery. J. Bacteriol. *192*, 6418–6427.
725 https://doi.org/10.1128/JB.00621-10.
726 35. Chimalapati, S., De Souza Santos, M., Servage, K., De Nisco, N.J., Dalia, A.B., and Orth, K.
727 (2018). Natural Transformation in *Vibrio parahaemolyticus* : a Rapid Method To Create
728 Genetic Deletions. J. Bacteriol. *200*. https://doi.org/10.1128/JB.00032-18.
729 36. Hershey, A.D., Kalmanson, G., and Bronfenbrenner, J. (1943). Quantitative methods in the
730 study of the phage-antiphage reaction. J. Immunol. *46*, 267–279.
731 https://doi.org/10.4049/jimmunol.46.5.267.
732 37. Sargen, M.R., Antine, S.P., Grabe, G.J., Antonellis, G., Ragucci, A.E., Li, Y., Kranzusch, P.J., and
733 Helaine, S. (2026). A prophage-encoded abortive infection protein preserves host and
734 prophage spread. Nature. https://doi.org/10.1038/s41586-025-10070-6.
735 38. Chiang, S.L., and Rubin, E.J. (2002). Construction of a mariner -based transposon for epitope-
736 tagging and genomic targeting. Gene *296*, 179–185. https://doi.org/10.1016/S0378-
737 1119(02)00856-9.
738 39. Truong, T.T., Vettiger, A., and Bernhardt, T.G. (2020). Cell division is antagonized by the activity
739 of peptidoglycan endopeptidases that promote cell elongation. Mol. Microbiol. *114*, 966–
740 978. https://doi.org/10.1111/mmi.14587.
741 40. Lan, S.-F., Huang, C.-H., Chang, C.-H., Liao, W.-C., Lin, I.-H., Jian, W.-N., Wu, Y.-G., Chen, S.-Y.,
742 and Wong, H.-C. (2009). Characterization of a new plasmid-like prophage in a pandemic *Vibrio*
743 *parahaemolyticus* O3:K6 strain. Appl. Environ. Microbiol. *75*, 2659–2667.
744 https://doi.org/10.1128/AEM.02483-08.

745 41. Makino, K., Oshima, K., Kurokawa, K., Yokoyama, K., Uda, T., Tagomori, K., Iijima, Y., Najima,
746 M., Nakano, M., Yamashita, A., et al. (2003). Genome sequence of *Vibrio parahaemolyticus:*
747 *a pathogenic* mechanism distinct from that of *V. cholerae*. The Lancet *361*, 743–749.
748 https://doi.org/10.1016/S0140-6736(03)12659-1.
749 42. Simon, R., Priefer, U., and Pühler, A. (1983). A broad host range mobilization system for in vivo
750 genetic engineering: Transposon mutagenesis in gram negative bacteria. Bio/Technology *1*,
751 784–791. https://doi.org/10.1038/nbt1183-784.
752 43. Sargen, M.R., and Helaine, S. (2024). A prophage competition element protects Salmonella
753 from lysis. Cell Host Microbe *32*, 2063-2079.e8. https://doi.org/10.1016/j.chom.2024.10.012.
754 44. Lan, S.-F., Huang, C.-H., Chang, C.-H., Liao, W.-C., Lin, I.-H., Jian, W.-N., Wu, Y.-G., Chen, S.-Y.,
755 and Wong, H. (2009). Characterization of a new plasmid-like prophage in a pandemic *Vibrio*
756 *parahaemolyticus* O3:K6 strain. Appl. Environ. Microbiol. *75*, 2659–2667.
757 https://doi.org/10.1128/AEM.02483-08.
758

759 **Figure Legends**

760

761 **Figure 1: Phage VP882 engages with both host quorum-sensing systems**

762 Both the *V. parahaemolyticus* VqmA-VqmR and LuxO QS systems influence the life cycle of phage

763 VP882 by both promoting lytic replication at high host cell densities. See text for details.

764

765 **Figure 2: The O3:K6 K-antigen is the phage VP882 receptor in *V. parahaemolyticus***

766 A) Diagram of transposon screen to identify genes encoding the phage VP882 receptor. B)

767 Quantitation of phage VP882 adsorption. Bacteria were incubated with phage VP882 lysate (final

768 MOI 10^{-3}-10^{-4}) for 20 min. Bacteria and adsorbed phage particles were separated from

769 unabsorbed (free) phage by centrifugation. Free phage were quantified by plaque assay on *V.*

770 *parahaemolyticus* cured of phage VP882. Percent free phage was calculated relative to a sample

771 lacking bacteria, and the value from that experiment was set to 100%. C) Phage VP882 plaque

772 formation on the designated strains. Ten-fold serial dilutions of phage VP882 lysate (starting at

773 10^{-8}-10^{-9} PFU/mL) were spotted on lawns of the indicated *V. parahaemolyticus* strains embedded

774 in 0.5% LB top agar overlaid onto 1.5% LB agar. Plaques were quantified after 16-20 h of

775 incubation at 37 °C. D) Diagram of *V. parahaemolyticus* 882 O- and K-antigen loci. The K-antigen

776 is encoded by *VP0215*-*VP0237* (blue). Transposon insertion sites are depicted as vertical lines

777 below genes. Black and red indicate insertions on the + and – strands, respectively. Genes shown

778 in black are markers that commonly flank O- and K-antigen loci in *V. parahaemolyticus* (from left

779 to right *coaD*, *gmhD*, and *rjg*). E and F) As in B and C, respectively, for the designated strains. G)

780 Table reporting *V. parahaemolyticus* serotypes, when known. + indicates plaques detected in 3

781 biological replicates. - indicates no plaques detected. H) As in C for the designated strains. col1
782 and col2 denote the translucent and opaque morphotypes, respectively. *VP0235+* indicates repair
783 of the frameshift in *VP0235*. I) As in B for the designated strains. In B, E, and I, data are presented
784 as means of 3 biological replicates and error bars denote SEMs. Significance was determined by
785 one-way ANOVA with Tukey's test for multiple comparisons to establish adjusted p-values. In C, F,
786 and H, a representative image from 3 biological replicates is shown.

787

788 **Figure 3: LuxO-driven quorum sensing controls phage VP882 infection**

789 A) Phage VP882 plaque formation on the designated phage-free strains, as in Figure 2C. B)
790 Quantification of plaque formation of phage VP882 on the designated strains from panel A.
791 Shown are the log differences in scores for phage VP882 clearance following infection of each
792 strain compared to that for infection on *V. parahaemolyticus* 882 (see Methods). C)
793 Bioluminescence output from P*luxC-luxCDABE* after 300 min of growth in LM at 30 °C of the
794 designated strains. Relative light units (RLU) are bioluminescence normalized to OD_{600}. D) Phage
795 VP882 plaque formation on the designated strains as in Figure 2C. E) Quantitation of phage
796 VP882$^{gp38::Cm}$ lysogens following infection of the designated phage-free strains (MOI 10^{-5}-10^{-6}). F)
797 Quantitation of phage VP882 adsorption as in Figure 2B. In B, C, E, and F, data are presented as
798 means of 3 biological replicates and error bars denote SEMs. Significance was determined by one-
799 way ANOVA with Tukey's test for multiple comparisons to determine adjusted p-values as
800 indicated. In B, the reported p-values above each bar specify comparisons to *V. parahaemolyticus*
801 882. In A and D, a representative image from 3 biological replicates is shown.

802

803 **Figure 4: VPA1602-VPA1604 are quorum-sensing-controlled components that shield *V.***
804 ***parahaemolyticus* from infection by phage VP882**

805 A) Quantitation of phage VP882 adsorption as in Figure 2B. B) Quantitation of phage VP882
806 lysogens as in Figure 3E. Data are presented as means of 3 biological replicates and error bars
807 denote SEMs. Significance was determined by one-way ANOVA with Tukey's test for multiple
808 comparisons to establish adjusted p-values. C) Diagram of *V. parahaemolyticus* K-antigen and the
809 putative extracellular polysaccharide that shields it.

810

811 **Figure 5: Superinfection of *V. parahaemolyticus* phage VP882 lysogens leads to phage VP882**
812 **genome recombination**

813 A) Phage VP882 plaque formation as in Figure 2C. A representative image from 3 biological
814 replicates is shown. B) Quantitation of phage VP882 adsorption as in Figure 2B. The phage used
815 for infection, phage VP882$^{\text{Ctr::Tn}5}$, does not produce functional virions that could interfere with
816 quantitation. C-E) Quantitation of phage VP882 lysogens as in Figure 3E except that in panels D
817 and E, phage VP882$^{gp38\text{::Gm}}$ was the infecting phage. In panel D, lysogens carried phage VP882$^{g71\text{-}}$
818 $^{\text{intergenic::Cm}}$. F) PCR products resulting from amplification of the *gp38* and *gp71*-intergenic loci in
819 the resident and infecting phage VP882 genomes and doubly-resistant superlysogens from the
820 experiment in Figure 5D. Diagrams depict the expected PCR product size for each locus in the
821 resident phage (VP882$^{g71\text{-intergenic::Cm}}$, green) and the infecting phage (VP882$^{gp38\text{::Gm}}$, black). 12-18
822 colonies were assayed in 3 biological replicates, and a representative gel is shown. In B, C, D, and

823 E, data are presented as means of 3 biological replicates and error bars denote SEMs. In B,
824 significance was determined by an unpaired t-test. In C, D, and E significance was determined by
825 one-way ANOVA with Tukey's test for multiple comparisons to establish adjusted p-values.

826

827 **Figure S1: Phage VP882 only infects *V. parahaemolyticus* with the O3:K6 K-antigen**

828 A and B) Colony morphologies of the designated phage-free *V. parahaemolyticus* 882 strains
829 grown on LB agar at 37 °C for 16 h. C) Growth curves of *V. parahaemolyticus* 882 carrying phage
830 VP882 or phage VP882$^{gp38::\mathrm{Cm}}$ treated with mitomycin C (0.05 µg/mL). A representative of 2
831 biological replicates is shown. Each assay included 2 technical replicates. D) Quantitation of phage
832 VP882$^{gp38::\mathrm{Cm}}$ lysogens following infection of the designated phage-free strains, as in Figure 3E
833 except that lysogenization was carried out for 16 h. E) Quantitation of phage VP882$^{gp38::\mathrm{Cm}}$
834 lysogens as in Figure 3E. F) Colony morphologies of the designated phage-free strains grown on
835 LB agar at 37 °C for 16 h. In A, B, and F, a representative image from 3 biological replicates is
836 shown. In C, D, and E, data are presented as means of 3 biological replicates and error bars
837 indicate SEMs. We note that in panel C, error bars are obscured by the symbols.

838

839 **Figure S2: VqmA-VqmR quorum sensing does not affect phage VP882 infection**

840 A) Quantitation of phage VP882 lysogens as in Figure 3E. B) Quantitation of phage VP882
841 adsorption as in Figure 2B. Data are presented as means of 3 biological replicates and error bars
842 indicate SEMs.

843

844 **Figure S3: *VPA1602-VPA1604* are controlled by the LuxO quorum-sensing system**

845 A) Heatmap showing quantitation of RNA-seq reads mapping to the *V. parahaemolyticus* K-
846 antigen locus for strains with the indicated QS genotypes after 4 h of growth in LM at 30 °C[20]. The
847 fraction of total reads aligning to each gene were normalized to the corresponding value for *V.*
848 *parahaemolyticus* 882. B) Quantitation of RNA-seq reads mapping to *VPA1602* from the
849 conditions described in A[20]. C) P*VPA1602-luxCDABE* output as in Figure 3C except measurements
850 were taken after 500 min. D and E) Quantitation of phage VP882 adsorption as in Figure 2B. F)
851 Quantitation of phage VP882 lysogens as in Figure 3E. G) Quantification of phage VP882 plaque
852 formation as in Figure 3B. For D-G, data are presented as means of 3 biological replicates and
853 error bars indicate SEMs. In C and D, significance was determined by one-way ANOVA with Tukey's
854 test for multiple comparisons to establish adjusted p-values.

855

856 **Figure S4: Phage VP882 genome recombination occurs during superlysogenization**

Diagram of phage VP882 genomes used to monitor recombination in the superinfection experiments reported in Figure 4D and F.

Table S1: Transposon insertion sites identified in the screen for the phage VP882 receptor.

Sequence Number	Insertion Site	Direction	Gene ID
1	231439	forward	*VP0220*
2	234489	forward	*VP0221*
3	234489	forward	*VP0221*
4	235609	forward	*VP0222*
5	235779	forward	*VP0222*
6	235855	forward	*VP0222*
7	235855	forward	*VP0222*
8	237039	forward	*VP0224*
9	243061	forward	*VP0230*
10	243498	reverse	*VP0231*
11	243643	forward	*VP0230*
12	243914	forward	*VP0230*
13	244073	forward	*VP0230*
14	244219	forward	*VP0231*
15	244285	forward	*VP0231*
16	244285	forward	*VP0231*
17	244479	forward	*VP0231*
18	249145	forward	*VP0235*
19	249360	reverse	*VP0235*

Table S2: Transposon insertion sites identified in the screen for the factor that prevents phage VP882 adsorption to *V. parahaemolyticus.*

Insertions in *VPA1602-4* are shaded gray

* indicates the read quality was too poor to identify the insertion site

Sequence Number	Insertion Site	Direction	Disrupted locus	Annotation
Chromosome 1				
1	77696	reverse	*VP0068*	*gorA*
2	92662	reverse	*VP0081*	BON Domain protein
3	183123	forward	*VP0168-VP0170*, intergenic	TonB-dependent receptor plug domain-containing protein and ABC transporter
4	102615	reverse	*VP0109*	*engB*
5	128809	reverse	*VP0120*	*glnL*
6	196839	reverse	*VP0183*	Methyl accepting chemotaxis protein
7	*	forward	*VP0199*	*neuC*
8	209620	forward	5' *VP0199*	5' of *neuC*
9	210461	forward	*VP0199*	*neuC*
10	253049	reverse	*VP0238*	MBL fold metallo-hydrolase
11	379167	forward,	5' *VP0377*	HTH domain protein
12	390779	forward	3' *VP0388*	methylase
13	426994	forward	*VP0424*	*hldE*
14	508389	forward	*VP0494*	*thrA*
15	545647	reverse	*VP0527*	*nhaR*
16	630725	forward	*VP0605*	rRNA large subunit methyltransferase N
17	681151	reverse	*VP06050, VP06051* intergenic	*nadK, grpE*
18	*	forward	*VP0682*	*ribH*
19	716483	forward	*VP0684*	*thiL*
20	827688	forward	5' *VP0793*	*crr*
21	*	reverse	*VP0831*	*nagE*
22	1022658	reverse	*VP0980*	DUF2062 domain protein
23	*	forward	*VP1231*	*fabV*
24	1386862	reverse	*VP1305/VP1306*	*cobU,* adenosylcobinamide-GDP ribazoletransferase
25	1421362	reverse	*VP1340*	Collagenase
26	2292011	reverse	3' *VP2183*	Response regulator

27	2549724	forward	*VP2429-VP2430,* intergenic	*radA*
28	2643101	forward	*VP2504*	*pcnB*
29	2688526	forward	5' *VP2546*	*csrA*
30	2688526	forward	5' *VP2546*	*csrA*
31	2723599	forward	*VP2577*	*rseA*
32	2723599	forward	*VP2577*	*rseA*
33	2755274	reverse	*VP2611*	*gshB*
34	2833881	forward	*VP2683*	PhoH family protein
35	2867011	forward	*VP2711*	*galU*
36	2971496	reverse	*VP2807*	*rnr*
37	3055472	forward	*VP2884*	*dusB*
38	3056590	forward	*VP2885*	*fis*
39	3056590	forward	*VP2885*	*fis*
40	3070488	reverse	*VPr018*	23S rRNA
41	3100523	forward	*VP2911*	5' of *hupA*
42	3220203	reverse	*VP3016*	HvfC/BufC N-terminal domain-containing protein
43	3247914	forward	*VP3041*	LysM domain protein
Chromosome 2				
44	37139	forward	*VPA0045*	Ada regulatory protein
45	44076	reverse	*VPA0063*	Hypothetical protein
46	452925	reverse	*VPA0495*	AraC family transcriptional regulator
47	*	forward	*VPA0627*	5' of *cyoA*
48	*	forward	*VPA1442*	DUF11 domain protein
48	1560611	forward	*VPA1464*	Lcl domain protein
49	1700868	forward	*VPA1602*	Polysaccharide export protein Wza
50	1700867	forward	*VPA1602*	Polysaccharide export protein Wza
51	1701292	reverse	*VPA1602*	Polysaccharide export protein Wza
52	1700403	forward	5' *VPA1602*	5' of *VPA1602* Polysaccharide export protein Wza
53	1799976	forward	*VPA1678*	*araC*
54	2932536	reverse	*VPA2764*	Homoserine dehydrogenase

Table S3: Strains used in this study

Identifier	Genotype	Plasmid/Phage	Source
V. parahaemolyticus 882			
MRS19		cured	This study, courtesy of O. Duddy
MRS21		VP882$^{gp71\text{-intergenic::Cm}}$	Duddy et al. 2023[20]
MRS34		VP882$^{ctr::Tn5}$	Silpe and Bassler 2019[6]
MRS70		VP882 (native)	Lan et al. 2009[40]
MRS138		Cured; pMRS7	This study
MRS187	*vqmR*$^{+}$-P *vqmA*$_{882}$- *vqmA*$_{882}$:: *vqmA*$_{882}$ (*vqmR-vqmA*882^{+})	cured	This study
MRS188	*luxO*882::*luxO*RIMD (*luxO*$^{+}$)	cured	This study
MRS189	*vqmR*$^{+}$-P*vqmA*$_{882}$- *vqmA*$_{882}$:: *vqmA*$_{882}$; *luxO*882::*luxO*$_{RIMD}$ (*vqmR-vqmA*882^{+} *luxO*$^{+}$)	cured	This study
MRS312	*luxO*$_{882}$::*luxO*^{D61E} (*luxO*^{D61E})	cured	This study
MRS313	*vqmR*$^{+}$-P*vqmA*$_{882}$-*vqmA*$_{882}$::*vqmA*$_{882}$; *luxO*$_{882:}$:*luxO*^{D61E} (*vqmR-vqmA*$_{882}$$^{+}$ *luxO*^{D61E})	cured	This study
MRS314	*luxO*$_{882}$::*luxO*^{D61A} (*luxO*^{D61A})	cured	This study
MRS417	*vqmR*$^{+}$-P*vqmA*$_{882}$-*vqmA*$_{882}$::*vqmA*$_{882}$; *luxO*$_{882:}$:*luxO*^{D61A} (*vqmR-vqmA*$_{882}$$^{+}$ *luxO*^{D61A})	cured	This study
MRS541		VP882 $^{gp38::Cm}$	This study
MRS542		VP882 $^{gp38::Gm}$	This study
MRS550	Δ*VPA1602-1604*	cured	This study
MRS551	*luxO*$_{882}$::*luxO*^{D61A} (*luxO*^{D61A}) Δ*galU*	cured	This study
MRS552	*luxO*$_{882}$::*luxO*^{D61A} (*luxO*^{D61A}) Δ*nagE*	cured	This study
MRS553	*luxO*$_{882}$::*luxO*^{D61A} (*luxO*^{D61A}) Δ*neuC*	cured	This study
MRS554	*luxO*$_{882}$::*luxO*^{D61A} (*luxO*^{D61A}) Δ*VPA1602-1604*	cured	This study
MRS566	*vqmR*$^{+}$-P *vqmA*$_{882}$-*vqmA*882:: *vqmA*$_{882}$ (*vqmR- vqmA*$_{882}$$^{+}$) Δ*VPA1602-1604*	cured	This study
MRS567	*luxO*882::*luxO*$_{RIMD}$ (*luxO*$^{+}$) Δ*VPA1602-1604*	cured	This study
MRS568	*luxO*$_{882}$::*luxO*^{D61E} (*luxO*^{D61E}) Δ*VPA1602-1604*	cured	This study
MRS569	*vqmR*$^{+}$-P*vqmA*$_{882}$-*vqmA*$_{882}$::*vqmA*$_{882}$; *luxO*$_{882:}$:*luxO*^{D61E} (*vqmR-vqmA*$_{882}$$^{+}$ *luxO*^{D61E}) Δ*VPA1602-1604*	cured	This study
MRS571	*vqmR*$^{+}$-P*vqmA*$_{882}$-*vqmA*$_{882}$::*vqmA*$_{882}$; *luxO*$_{882:}$:*luxO*^{D61A} (*vqmR-vqmA*$_{882}$$^{+}$ *luxO*^{D61A}) Δ*VPA1602-1604*		This study
MRS574	*vqmR*$^{+}$-P*vqmA*$_{882}$-*vqmA*$_{882}$::*vqmA*$_{882}$; *luxO*882::*luxO*$_{RIMD}$ (*vqmR- vqmA*$_{882}$$^{+}$ *luxO*$^{+}$) Δ*VPA1602-1604*		
MRS703	Δ*VPA1602-1604*	VP882 (native)	This study
MRS707	*luxO*$_{882}$::*luxO*^{D61A} (*luxO*^{D61A}) Δ*VPA1602-1604*	VP882 (native)	This study
MRS759	Δ*VP0230*	cured	This study
MRS769		VP882 (native); FJS-P073	This study
MRS770	*luxO*882::*luxO*$_{RIMD}$ (*luxO*$^{+}$)	VP882 (native); FJS-P073	This study
MRS806		cured; pMRS70	This study

MRS812	*luxO*$_{882}$::*luxO*^{D61A} (*luxO*^{D61A})	cured; pMRS70	This study
MRS956	*luxO*$_{882}$::*luxO*^{D61A} (*luxO*^{D61A}) Δ*VP0235*		This study
MRS958	Δ*VPA1602-4 ΔVP0235*		This study
MRS959	*luxO*$_{882}$::*luxO*^{D61A} (*luxO*^{D61A}) Δ*VPA1602-1604* Δ*VP0235*		This study
MRS970	Δ*recA*	cured	This study
MRS976	Δ*recA*	VP882 (native)	This study
MRS1011	Δ*recA*	VP882$^{gp71\text{-intergenic::Cm}}$	This study
V. parahaemolyticus VP81			
MRS729	col1		ATCC
MRS730	col2		ATCC
MRS758	col2 *VP0235*$^{+}$		This study
V. parahaemolyticus VP47			
MRS743			ATCC
MRS777	*luxO*$^{+}$		This study
MRS775		FJS-P073	This study
MRS778	*luxO*$^{+}$	FJS-P073	This study
Other *V. parahaemolyticus*			
MRS8	*V. parahaemolyticus* RIMD2210633		Makino et al.[41]
MRS733	*V. parahaemolyticus* VP232		ATCC
MRS734	*V. parahaemolyticus* EB101		ATCC
MRS735	*V. parahaemolyticus* 954		ATCC
MRS736	*V. parahaemolyticus* 205		ATCC
MRS737	*V. parahaemolyticus* 03/4 K30		ATCC
MRS738	*V. parahaemolyticus* 117		ATCC
MRS739	*V. parahaemolyticus* 115		ATCC
MRS740	*V. parahaemolyticus* MDL 3875-7-83		ATCC
MRS741	*V. parahaemolyticus* 10884		ATCC
MRS742	*V. parahaemolyticus* VP250		ATCC
MRS744	*V. parahaemolyticus* FC 1011		ATCC
E. coli strains for cloning and conjugative donors			
E. coli MFDλpir	MG1655 RP4-2-Tc::[ΔMu1::*aac(3)IV*-Δ*aphA*-Δ*nic*35 ΔMu2::*zeo*] Δ*dapA*::(*erm-pir*) Δ*recA*		Ferrières et al. 2010[34]
E. coli S17λ*pir*	Δ*lacU169 (ΦlacZΔM15) recA1 endA1 hsdR17 thi-1 gyrA96 relA1 λpir*		Simon et al. 1983[42]
E. coli TOP10	F- *mcrA* Δ(*mrr-hsdRMS-mcrBC*) Φ80*lacZΔM15* Δ*lacX74 recA1 araD139* Δ(*ara leu*)*7697 galU galK rpsL* (Str^{R}) *endA1 nupG*		Invitrogen
E. coli pir2^{+}	F^{-} Δ*lac*169 *rpo*S(am) *rob*A1 *cre*C510 *hsd*R514 *end*A *rec*A1 *uidA(ΔMlu*I*)*::*pir*		Invitrogen

Table S4: Oligonucleotides used in this study

Identifier	Name	Sequence (5'-3')	Purpose	Source
oMRS1	*qtip*-exR	CCGAAGAAAGCGCAGAAGC	check for presence of phage VP882	This study
oMRS2	VP882-*vqmA*-exR	TGCAATTTGTCGAGAAGGATGC	check for presence of phage VP882	This study
oMRS29	pRE1128-pTOXconvert-F	GTTTAAACCAGGTTAATTAATTTGAGAAGCGGTGTAAGTGAACTG	transfer pRE112 insert to pTOX	This study
oMRS30	pRE1128-pTOXconvert-R	CTCGAGACGTCCCGGGATGCATTTTCTTCTAGAGGTACCGCATGC	transfer pRE112 insert to pTOX	This study
oMRS138	Arb1D	GGCCAGGCCTGCAGATGATGNNNNNNNNNNGTAT	Mariner transposon insertion site identification	Truong et al. 2020[39]
oMRS139	Arb2	GGCCAGGCCTGCAGATGATG	Mariner transposon insertion site identification	Truong et al. 2020[39]
oMRS140	Neo-F	CGTTGGCTACCCGTGATATT	Mariner transposon insertion site identification	Truong et al. 2020[39]
oMRS141	pSC189-1st-3	GGCTGACCGCTTCCTCGTGCTTTAC	Mariner transposon insertion site identification	Truong et al. 2020[39]
oMRS142	*vqmA*host-outer_fwd	ACGCATTTCCTGTACCAGCA	check *vqmRA* of Vpara	This study, courtesy of T.V.P. Nguyen
oMRS143	*vqmA*host-outer_rev	AAGCGATTGGTTTGTTGCGT	check *vqmRA* of Vpara	This study, courtesy of T.V.P. Nguyen
oMRS194	d*VP0235*_downR	TCTTCTAGAGGTACCGCATGCGAATCCAGCTCATTAAAGTATGC	construction of pTOX plasmid for deletion	This study
oMRS195	d*VP0235*_ovF	ATATGGCAACTTGACGCTATACAATTTATGAGTCAATC	construction of pTOX plasmid for deletion	This study
oMRS196	d*VP0235*_ovR	ATAGCGTCAAGTTGCCATATAAATTGTAGACGTTGC	construction of pTOX plasmid for deletion	This study
oMRS197	d*VP0235*_upF	GTAAGTGAACTGCATGAATTCCCGGAATCGATACACGCAGTACTG	construction of pTOX plasmid for deletion	This study
oMRS198	*VP0235*-ex-F	ACGGGAAGTATTGTTGTTAGCTC	check deletion	This study
oMRS199	*VP0235*-ex-R	GACTTCCACAACAAGTAGAATAACC	check deletion	This study
oMRS225	*0230*_downR	CTCGAGACGTCCCGGGATGCATTTACACTACAACTGCCATCATAAGG	construction of pTOX plasmid for deletion	This study
oMRS226	*0230*_upF	GTTTAAACCAGGTTAATTAATTTTTTCTGCATATTCGGTTTGGTTCG	construction of pTOX plasmid for deletion	This study
oMRS231	d*0230*_ovR	TCACCGCCTCAAAGTACTGATGAAGGTATAAAAC	construction of pTOX plasmid for deletion	This study
oMRS232	d*0230*_ovF	TCAGTACTTTGAGGCGGTGAGTGATGAAAAG	construction of pTOX plasmid for deletion	This study
oMRS233	*luxO*vph-ex-F2	GAGGGGTCGCTAATATATCAG	check *luxO* sequence	This study
oMRS27	oMS714	CTGCGCCATCAGATCCTTGG	check insert in pTOX	Sargen and Helaine 2024[43]
oMRS28	oMS715	CGATATCTTCGAACCGGTGC	check insert in pTOX	Sargen and Helaine 2024[43]
oMRS72	*luxO*vph-ex-R	TCAAATACATTAAGCGCTCTGAACC	check genotype	This study
oMRS310	pEVS*lux*_RBS_vectorF	GCTTAACTAAGTAACTAGTACAGG	PCR of pEVS-lux backbone	This study
oMRS311	pEVS*lux*_vector_R	TTAATTAACTCGAGCGGTACC	PCR of pEVS-lux backbone	This study

oMRS409	*gp38*_gm_ovR	GAGAGTAGGGAACTGCCAGGTAGGATCTCCGTTTACCAGTTATAAAT	construction of gentamicin marked *gp38* phage	This study
oMRS410	*gp38*_gm_ovF	ACCCAAGTACCGCCACCTAAAAAAGCCCGCACAAGGCGG	construction of gentamicin marked *gp38* phage	This study
oMRS411	gm_cassette_R	TTAGGTGGCGGTACTTGGGTC	construction of gentamicin marked *gp38* phage	This study
oMRS412	gm_cassette_F	CCTGGCAGTTCCCTACTC	construction of gentamicin marked gp38 phage	This study
oMRS445	*galU*_upF	GTTTAAACCAGGTTAATTAATTTTCTGCAGATTATGTTGTGATTGC	construction of pTOX plasmid for deletion	This study
oMRS446	*galU*_downR	CTCGAGACGTCCCGGGATGCATTTCACTTGGTAAACAATGTTATCTGC	construction of pTOX plasmid for deletion	This study
oMRS447	d*galU*_ovR	GCCTGAACAATTTTAAATTCACCAACTGTAAAAAAGG	construction of pTOX plasmid for deletion	This study
oMRS448	d*galU*_ovF	GAATTTAAAATTGTTCAGGCTCGTTACCAATG	construction of pTOX plasmid for deletion	This study
oMRS449	*nagE*_upF	GTTTAAACCAGGTTAATTAATTTTCAACGCTATGAATACCTTTTTTCG	construction of pTOX plasmid for deletion	This study
oMRS450	*nagE*_downR	CTCGAGACGTCCCGGGATGCATTTGGCTGAACTCGTATTGATGAGG	construction of pTOX plasmid for deletion	This study
oMRS451	d*nagE*_ovR	TTCGATGTAACTTAAGTTCCCCCTATAGGATTC	construction of pTOX plasmid for deletion	This study
oMRS452	d*nagE*_ovF	GGAACTTAAGTTACATCGAACTAATATTTGATTAGAGAC	construction of pTOX plasmid for deletion	This study
oMRS453	*neuC*_upF	GTTTAAACCAGGTTAATTAATTTTACGTAATGGAAACGATTGAGAG	construction of pTOX plasmid for deletion	This study
oMRS454	*neuC*_downR	CTCGAGACGTCCCGGGATGCATTTCCAGAGCCAGGACGTTTAATCG	construction of pTOX plasmid for deletion	This study
oMRS455	d*neuC*_ovR	AATCAGGTTCAACCGCGACCTTTTTCTGTGTC	construction of pTOX plasmid for deletion	This study
oMRS456	d*neuC*_ovF	GGTCGCGGTTGAACCTGATTTAAATAAGAAAGTAGAG	construction of pTOX plasmid for deletion	This study
oMRS457	*VPA16024*_upF	GTTTAAACCAGGTTAATTAATTTGCTCAAAACTGCTTACTGGCAG	construction of pTOX plasmid for deletion	This study
oMRS458	*VPA16024*_downR	CTCGAGACGTCCCGGGATGCATTTATGGCGAAATTATTGCAAGTTGATTTTG	construction of pTOX plasmid for deletion	This study
oMRS459	d*VPA16024*_ovR	CTAGATTAATGTTTTTTCATTCATCTGACGTAAAGAG	construction of pTOX plasmid for deletion	This study
oMRS460	d*VPA16024*_ovF	ATGAAAAAACATTAATCTAGATCGCTAATTTGACC	construction of pTOX plasmid for deletion	This study
oTN0155	P*cat-cat*_fwd	TGATCGGCACGTAAGAGGTTCCAACTTTC	construction of phages marked at *gp38*	This study, courtesy of T.V.P. Nguyen
oTN0156	P*cat-cat*_rev	TTACGCCCCGCCCTGCCA	construction of phages marked at *gp38*	This study, courtesy of T.V.P. Nguyen
oTN0157	upstream-*gp38*_fwd	AGCACGTTGACCAGTCCG	construction of phages marked at *gp38*	This study, courtesy of T.V.P. Nguyen
oTN0158	upstream-*gp38*_rev	ACTGCGATGAGTGGCAGGGCGGGGCGTAATAGGATCTCCGTTTACCAGTTATAAATAATC	construction of phages marked at *gp38*	This study, courtesy of T.V.P. Nguyen
oTN0159	downstream-*gp38*_fwd	GAAAGTTGGAACCTCTTACGTGCCGATCAAAAAGCCCGCACAAGGCG	construction of phages marked at *gp38*	This study, courtesy of T.V.P. Nguyen
oTN0160	downstream-*gp38*_rev	GGACGACTATCGCGGCCA	construction of phages marked at *gp38*	This study, courtesy of T.V.P. Nguyen
oTN0161	delta*gp38*-cmR_fwdcmR_fwd	CGACGAGACGGACATGAGTT	construction of phages marked at *gp38*	This study, courtesy of T.V.P. Nguyen

oTN0162	deltagp38-cmR_rev	deltagp38-cmR_rev	construction of phages marked at *gp38*	This study, courtesy of T.V.P. Nguyen
oTN0169	*gp38*_fwd	GACGGTGAAGGGTAAGGTGG	PCR of *gp38* locus	This study, courtesy of T.V.P.Nguyen
oTN0170	*gp38*_rev	GTCCGTCCTCCTATTTGCCC	PCR of *gp38* locus	This study, courtesy of T.V.P. Nguyen
oMRS598	P*1602*_F3	TTAATACAACGAGATAATTAGTCGG	construction of pMRS70	This study
oMRS599	P*1602*_R2	GCTGGTAGCAACATTCTTCTC	construction of pMRS70	This study
oMRS630	GAB199	AGGTATGGAAGAAGGGACTCG	PCR of *gp71*-intergenic locus	This study, courtesy of G. Beggs
oMRS631	GAB200	CGTCTATTACTTCGCTATCGGATG	PCR of *gp71*-intergenic locus	This study, courtesy of G. Beggs
oMRS179	pRE112-primer2-ext	CCAATTCTGAGGGATCGGGCCCTATCACTT	construction of pBAD-q-Cm^R	This study
oMRS180	pRE112-Pcat-F	AAGGGGTGTTTCCTGGTGTCCCTGTTGATAC	construction of pBAD-q-Cm^R	This study
oMRS181	pJES-093-primer2-R	GCCCGATCCCTCAGAATTGGTTAATTGGTTGTAAC	construction of pBAD-q-Cm^R	This study
oMRS182	pJES-093-ab-F	GACACCAGGAAACACCCCTTGTATTACTGTTTATG	construction of pBAD-q-Cm^R	This study

Table S5: Plasmids used in this study

Identifier	Description	Backbone	Marker	Origin	Construction	Source
pMRS1	pRE112-*VqmA*$_{Vpara}$-ΔFLAG	pRE112	Cm	R6λγpir	Gibson assembly, SmaI site	This study
pMRS3	pTOX2-*VqmA*$_{Vpara}$-ΔFLAG	pTOX2	Cm	R6λγpir	Gibson assembly, SwaI site	This study
pMRS7	pBAD-*q*(CmR)	pEVS	Cm	p15A	Gibson assembly	This study
pMRS12	pTOX2-*VP0235*$^{+}$	pTOX2	Cm	R6λγpir	Gibson assembly, SwaI site	This study
pMRS13	pTOX2-*ΔVP0235*	pTOX2	Cm	R6λγpir	Gibson assembly, SwaI site	This study
pMRS19	pTOX2-Δ*VP0230*	pTOX2	Cm	R6λγpir	Gibson assembly, SwaI site	This study
pMRS22	pTOX2-Δ*recA*	pTOX2	Cm	R6λγpir	FastCloning, SwaI site	This study
pMRS27	pTOX2-Δ*galU*	pTOX2	Cm	R6λγpir	Gibson assembly, SwaI site	This study
pMRS28	pTOX2-Δ*nagE*	pTOX2	Cm	R6λγpir	Gibson assembly, SwaI site	This study
pMRS29	pTOX2-Δ*neuC*	pTOX2	Cm	R6λγpir	Gibson assembly, SwaI site	This study
pMRS30	pTOX2-Δ*VPA1602-1604*	pTOX2	Cm	R6λγpir	Gibson assembly, SwaI site	This study
pMRS70	pEVS-P*VPA1602*(1)-*luxCDABE*	pEVS (Ec1508)	Kan	p15A	FastCloning	This study
FJS-P073	pEVS-P*luxC-luxCDABE*	pEVS	Kan	p15A	X	Santoriello and Bassler 2024[23]
pOD-51	pRE112- *luxO*$_{882}$::*luxO*$_{RIMD}$	pRE112	Cm	R6λγpir	X	Duddy et al. 2023[20]
pSC189	Mariner transposon delivery		Kan/ Amp	R6λγpir	X	Chiang et al. 2002[38]
pMMB-tfoX-sacB	Natural transformation of *V. parahaemolyticus*	pMMB	Kan	pMMB	X	Chimalapati et al. 2018[35]
Plasmid-Phages						
	VP882 (native)	VP882	X	RepA	WT	Lan et al. 2009[44]
MRS-P28	VP882 ^{gp38}::Cm	VP882	Cm	RepA	Natural transformation	This study, courtesy of T.V.P. Nguyen.
MRS-P29	VP882^{gp38}::Gm	VP882	Gm	RepA	Natural transformation	This study
	VP882^{gp71}-intergenic::Cm	VP882	Cm	RepA	Natural transformation	Duddy et al. 2023[20]
	VP882^{ctr}::Tn*5*	VP882	Cm	RepA	Natural transformation	Silpe and Bassler, 2019[6]
MRS-P12	VP882^{gp59}(ΔP98-L120fs)	VP882	X	RepA	Spontaneous frameshift in cI	This study

Figure 1

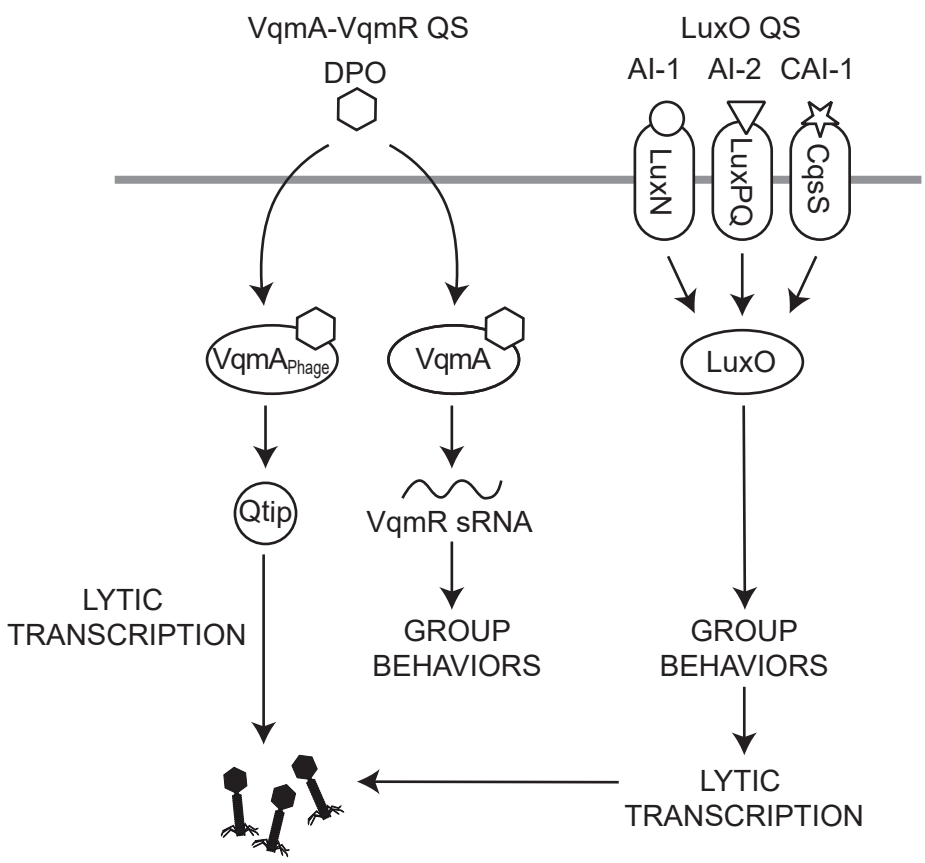
VqmA-VqmR QS
DPO
LuxO QS
AI-1
AI-2
CAI-1
LuxN
LuxPQ
CqsS
VqmA Phage
VqmA
LuxO
Qtip
VqmR sRNA
LYTIC TRANSCRIPTION
GROUP BEHAVIORS
GROUP BEHAVIORS
LYTIC TRANSCRIPTION

Figure 2

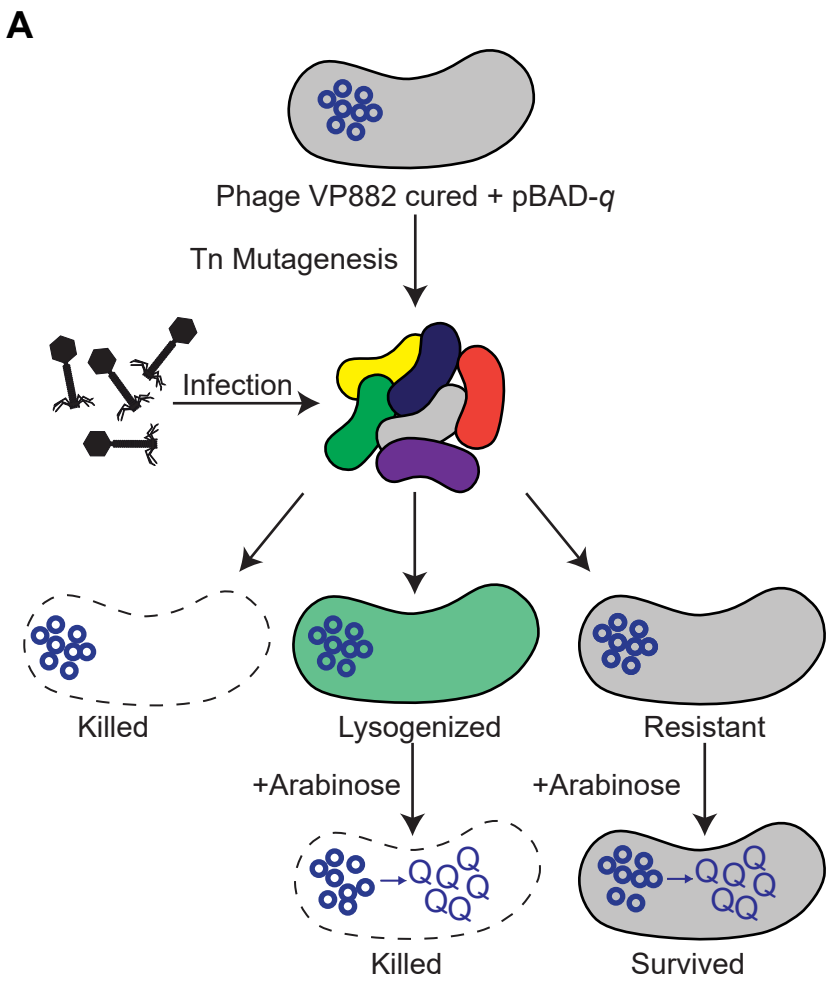

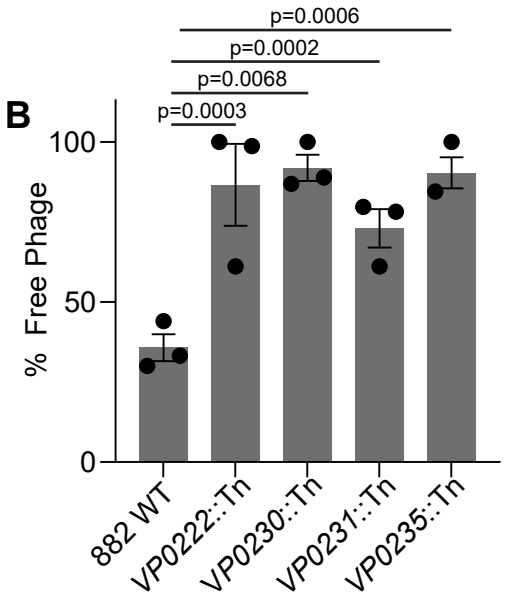

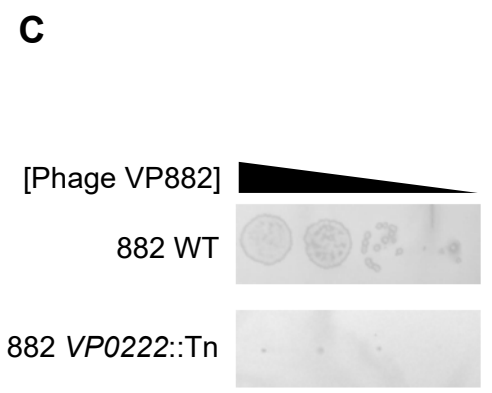

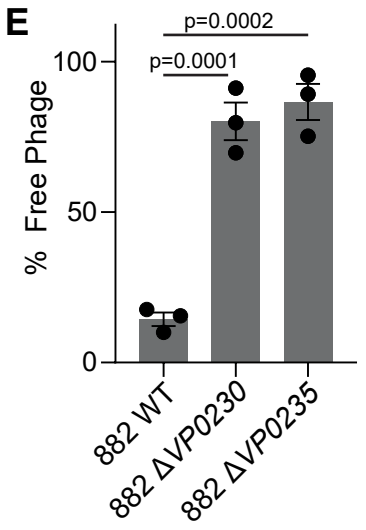

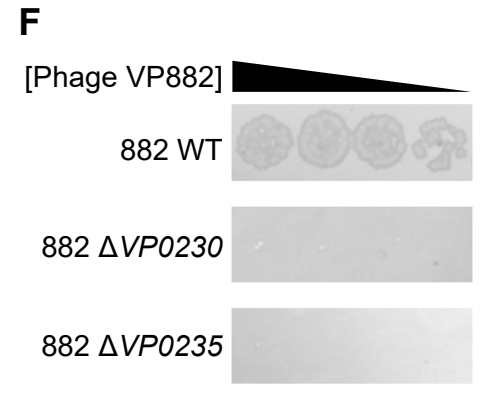

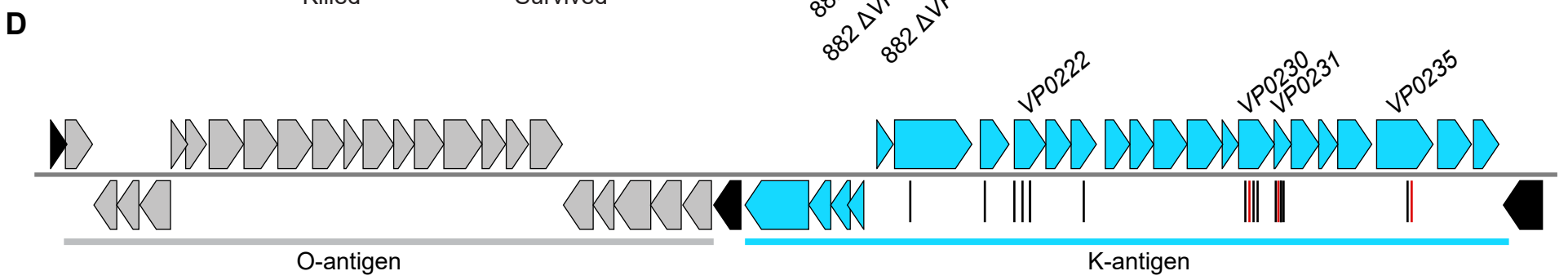

G

Strain	Serotype	Plaquing
882	O3:K6	+
RIMD	O3:K6	+
VP81-col1	O3:K6	+
VP81-col2	O3:K6	-
VP47	O3:K6	+
VP232	O4:K68	-
EB101	undetermined	-
954	not specified	-
205 [9302]	not specified	-
03/4 K30	not specified	-
117 [CDC KC830]	not specified	-
115 [CDC KC824]	not specified	-
MDL 3875-7-83	O4:K12	-
NCTC10884	not specified	-
VP250	O1:KUT	-
FC 1011	not specified	-

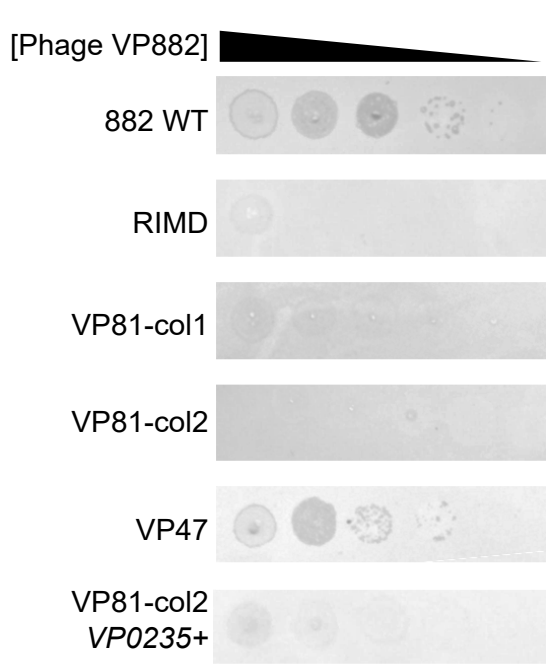

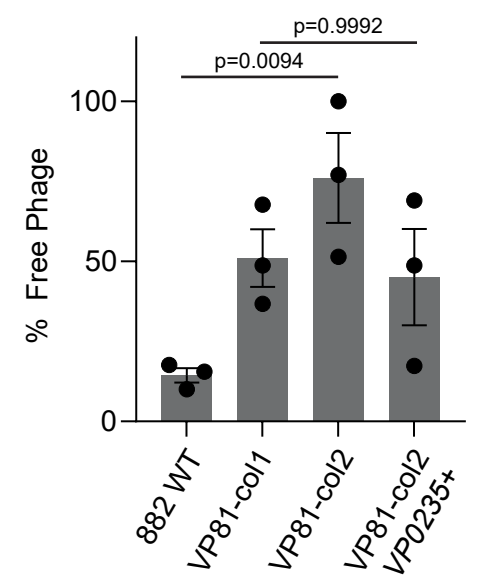

Figure 3

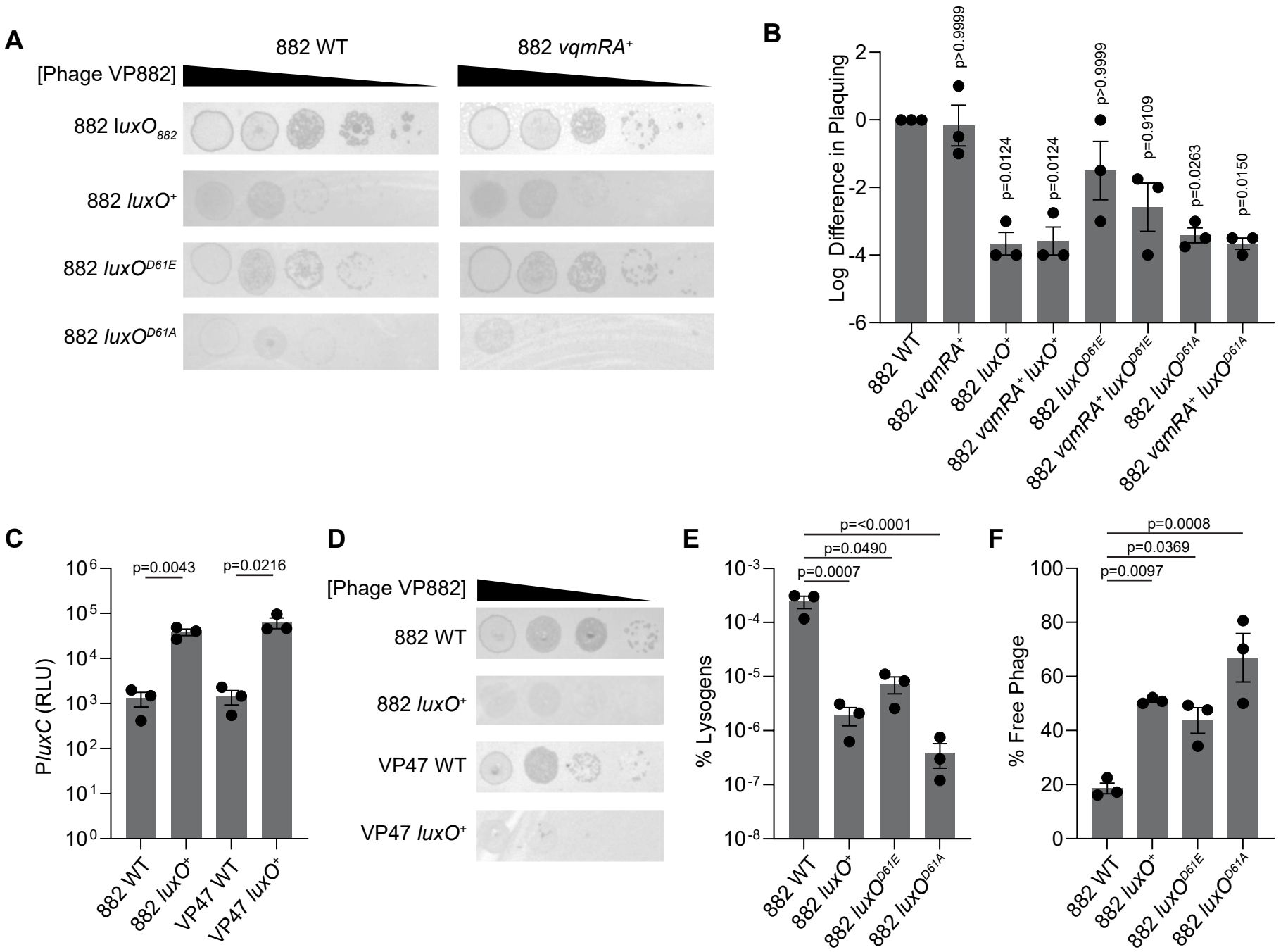
A
882 WT
882 vqmRA+
[Phage VP882]
882 luxO882
882 luxO+
882 luxOD61E
882 luxOD61A
B
Log Difference in Plaquing
p>0.9999
p=0.0124
p=0.0124
p>0.9999
p=0.9109
p=0.0263
p=0.0150
882 WT
882 vqmRA+
882 luxO+
882 vqmRA+ luxO+
882 luxOD61E
882 vqmRA+ luxOD61E
882 luxOD61A
882 vqmRA+ luxOD61A
C
PluxC (RLU)
p=0.0043
p=0.0216
882 WT
882 luxO+
VP47 WT
VP47 luxO+
D
[Phage VP882]
882 WT
882 luxO+
VP47 WT
VP47 luxO+
E
% Lysogens
p=<0.0001
p=0.0490
p=0.0007
882 WT
882 luxO+
882 luxOD61E
882 luxOD61A
F
% Free Phage
p=0.0008
p=0.0369
p=0.0097
882 WT
882 luxO+
882 luxOD61E
882 luxOD61A

Figure 4

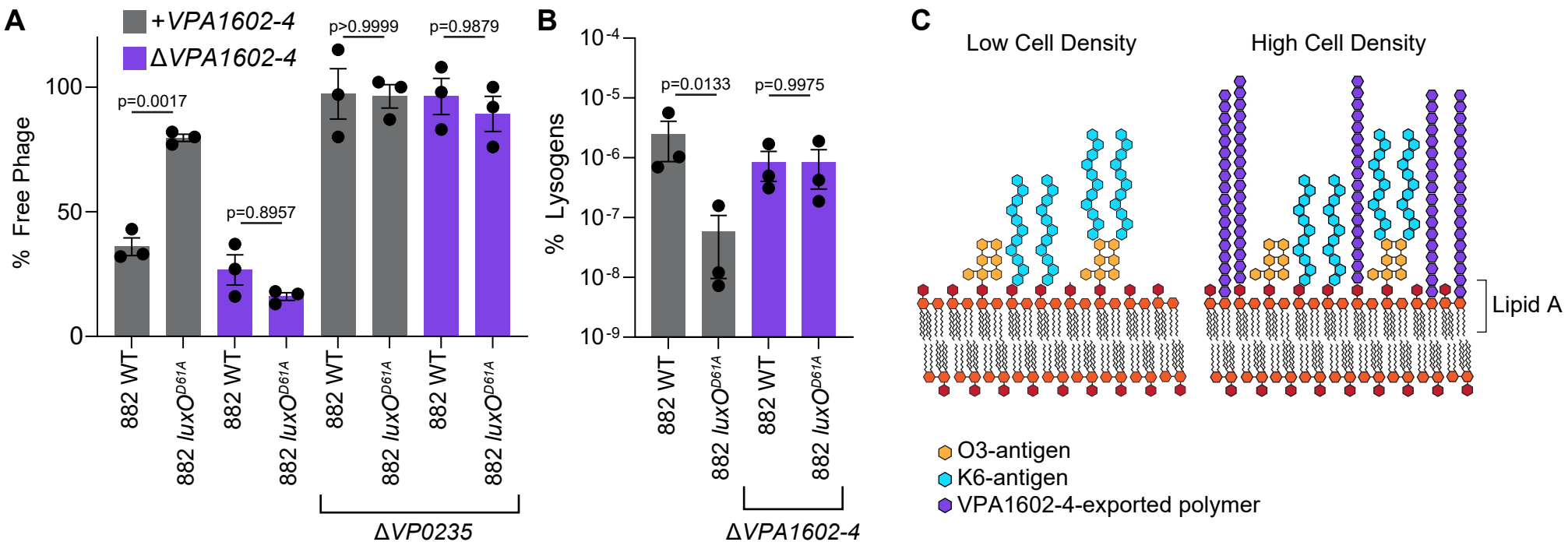
A
+VPA1602-4
ΔVPA1602-4
% Free Phage
100
50
0
p=0.0017
p=0.8957
p>0.9999
p=0.9879
882 WT
882 luxO^D61A
882 WT
882 luxO^D61A
882 WT
882 luxO^D61A
882 WT
882 luxO^D61A
ΔVP0235
B
% Lysogens
10^-4
10^-5
10^-6
10^-7
10^-8
10^-9
p=0.0133
p=0.9975
882 WT
882 luxO^D61A
882 WT
882 luxO^D61A
ΔVPA1602-4
C
Low Cell Density
High Cell Density
Lipid A
O3-antigen
K6-antigen
VPA1602-4-exported polymer

Figure 5

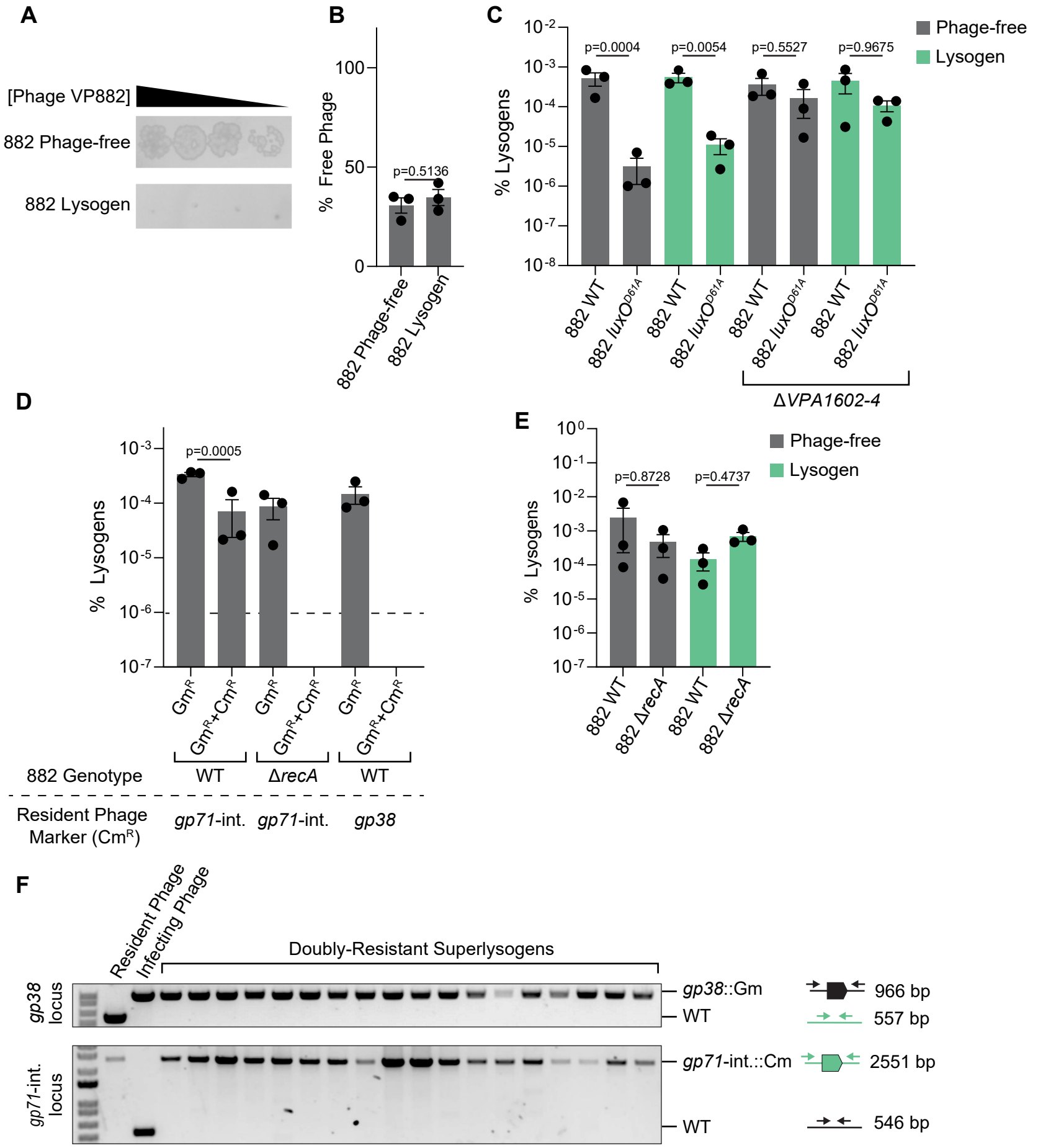
A
[Phage VP882]
882 Phage-free
882 Lysogen
B
% Free Phage
100
50
0
p=0.5136
882 Phage-free
882 Lysogen
C
% Lysogens
Phage-free
Lysogen
p=0.0004
p=0.0054
p=0.5527
p=0.9675
882 WT
882 luxO^D61A
ΔVPA1602-4
D
% Lysogens
p=0.0005
Gm^R
Gm^R+Cm^R
882 Genotype
WT
ΔrecA
Resident Phage Marker (Cm^R)
gp71-int.
gp38
E
% Lysogens
Phage-free
Lysogen
p=0.8728
p=0.4737
882 WT
882 ΔrecA
F
Resident Phage
Infecting Phage
Doubly-Resistant Superlysogens
gp38 locus
gp71-int. locus
gp38::Gm
WT
gp71-int.::Cm
966 bp
557 bp
2551 bp
546 bp

Figure S1

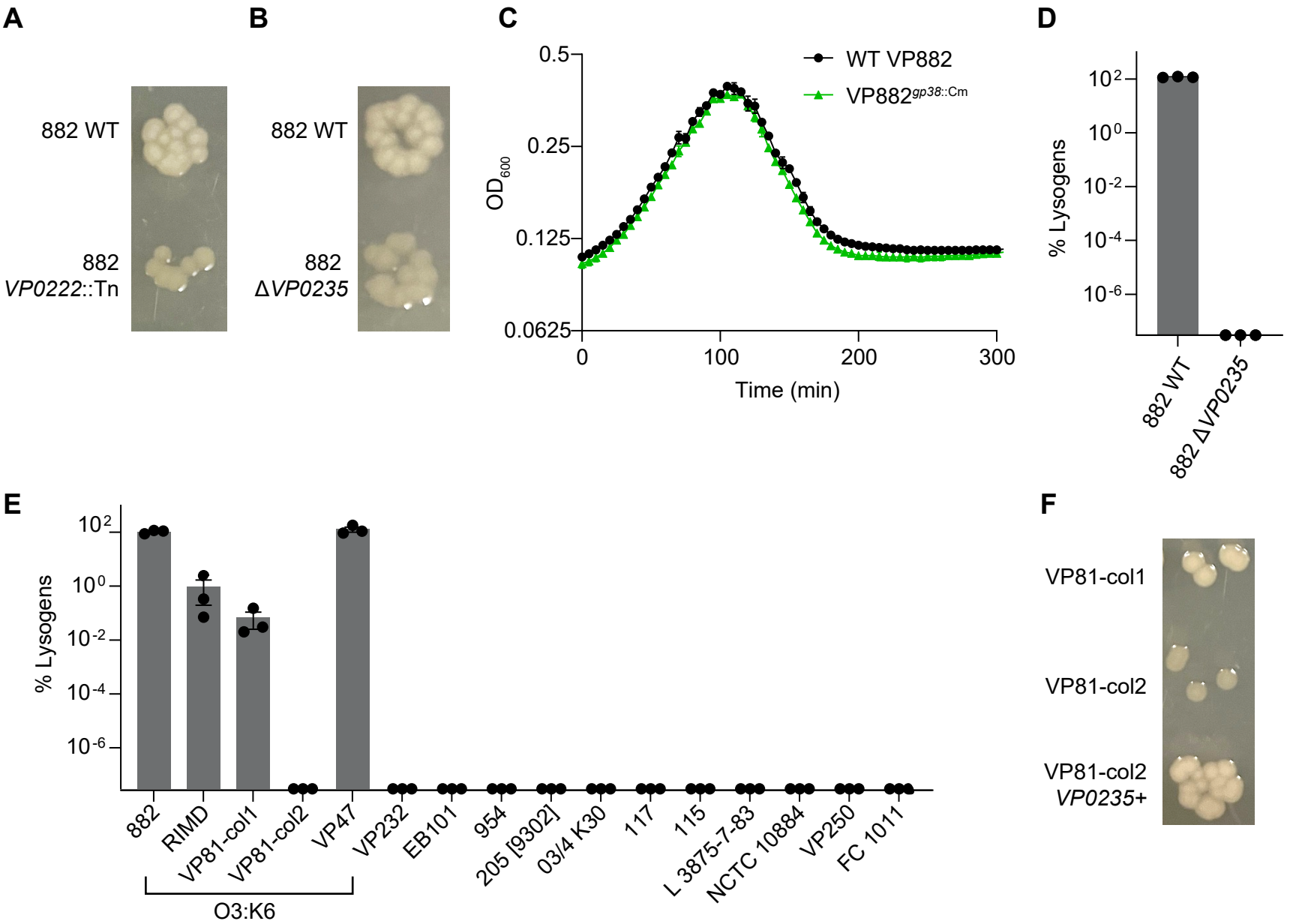
A
882 WT
882
VP0222::Tn
B
882 WT
882
ΔVP0235
C
WT VP882
VP882gp38::Cm
OD600
0.5
0.25
0.125
0.0625
0
100
200
300
Time (min)
D
% Lysogens
10^2
10^0
10^-2
10^-4
10^-6
882 WT
882 ΔVP0235
E
% Lysogens
10^2
10^0
10^-2
10^-4
10^-6
882
RIMD
VP81-col1
VP81-col2
VP47
VP232
EB101
954
205 [9302]
03/4 K30
117
115
L 3875-7-83
NCTC 10884
VP250
FC 1011
O3:K6
F
VP81-col1
VP81-col2
VP81-col2
VP0235+

Figure S2

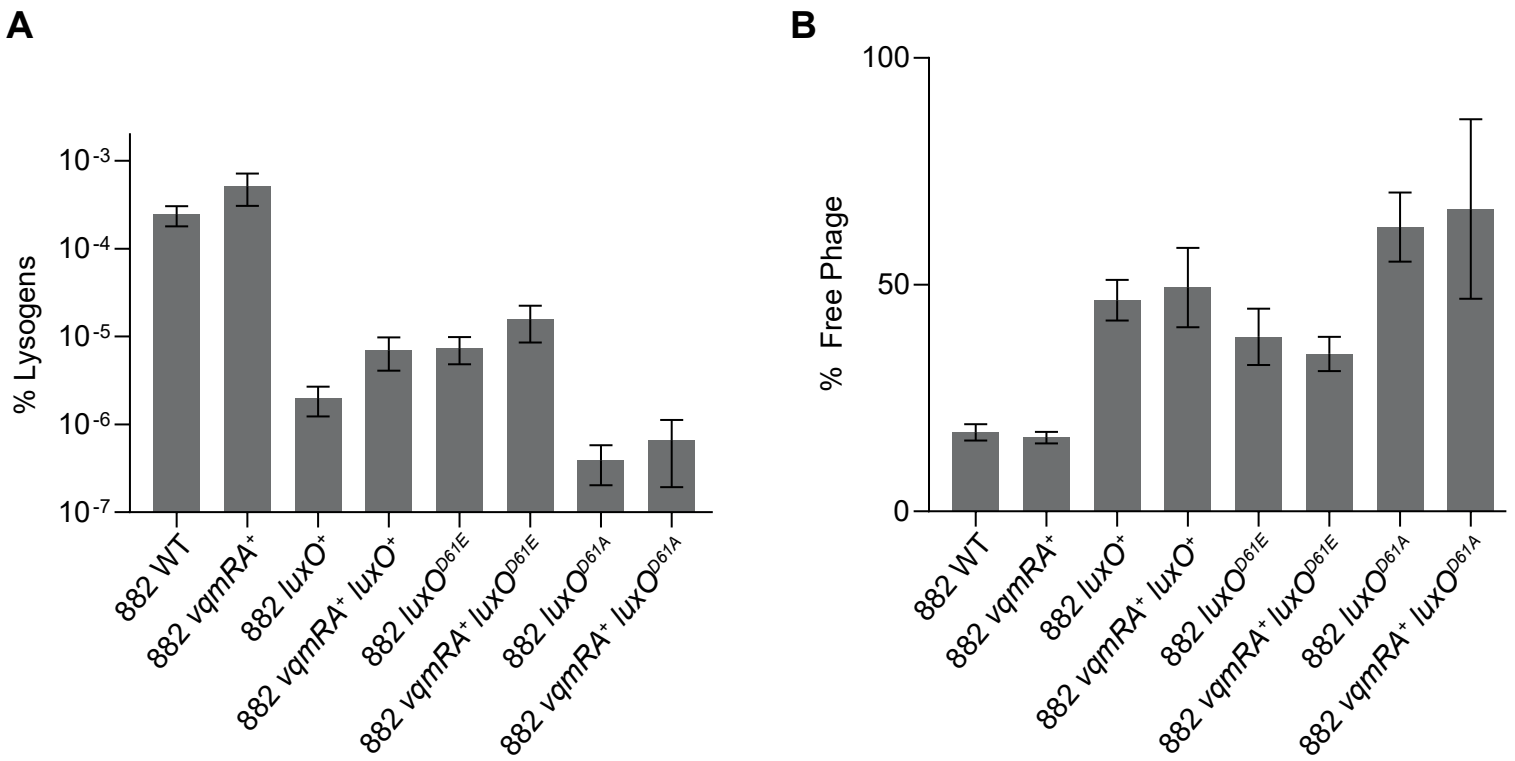
A
% Lysogens
10-3
10-4
10-5
10-6
10-7
882 WT
882 vqmRA+
882 luxO+
882 vqmRA+ luxO+
882 luxOD61E
882 vqmRA+ luxOD61E
882 luxOD61A
882 vqmRA+ luxOD61A
B
% Free Phage
100
50
0
882 WT
882 vqmRA+
882 luxO+
882 vqmRA+ luxO+
882 luxOD61E
882 vqmRA+ luxOD61E
882 luxOD61A
882 vqmRA+ luxOD61A

Figure S3

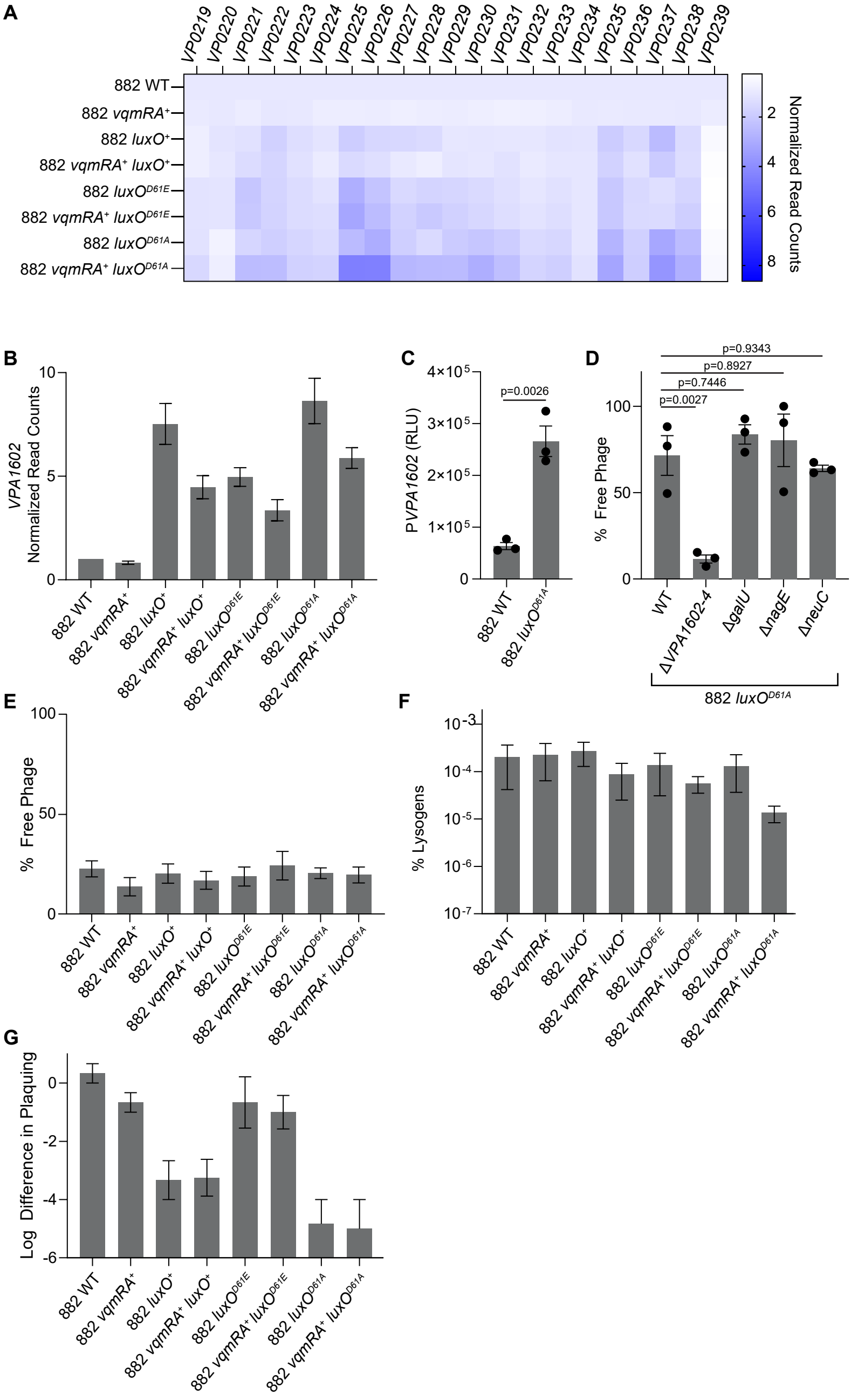
A
VP0219
VP0220
VP0221
VP0222
VP0223
VP0224
VP0225
VP0226
VP0227
VP0228
VP0229
VP0230
VP0231
VP0232
VP0233
VP0234
VP0235
VP0236
VP0237
VP0238
VP0239
882 WT
882 vqmRA+
882 luxO+
882 vqmRA+ luxO+
882 luxOD61E
882 vqmRA+ luxOD61E
882 luxOD61A
882 vqmRA+ luxOD61A
Normalized Read Counts
2
4
6
8
B
VPA1602 Normalized Read Counts
10
5
0
C
PVPA1602 (RLU)
4×10^5
3×10^5
2×10^5
1×10^5
0
p=0.0026
D
% Free Phage
100
50
0
p=0.9343
p=0.8927
p=0.7446
p=0.0027
WT
ΔVPA1602-4
ΔgalU
ΔnagE
ΔneuC
882 luxOD61A
E
% Free Phage
100
50
0
F
% Lysogens
10^-3
10^-4
10^-5
10^-6
10^-7
G
Log Difference in Plaquing
0
-2
-4
-6

Figure S4

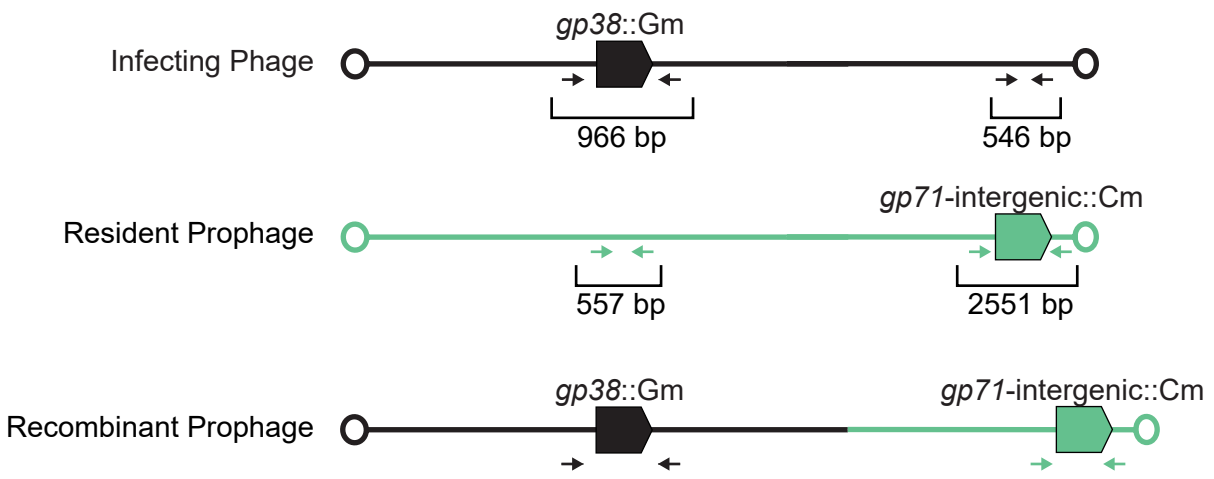
Infecting Phage
gp38::Gm
966 bp
546 bp
Resident Prophage
gp71-intergenic::Cm
557 bp
2551 bp
Recombinant Prophage
gp38::Gm
gp71-intergenic::Cm